CR-54942

CONTROL DYNAMICS ANALYSIS OF THE CENTAUR STAGE PROPELLANT UTILIZATION CONTROL SYSTEM

GD|C-DDE65-007

May 1965

Prepared Under

Contract NAS3-3232

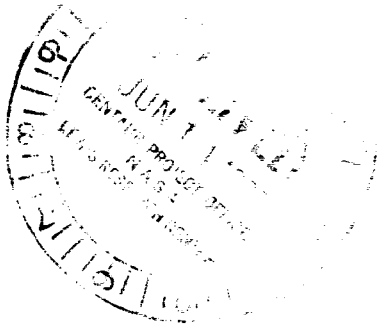

GENERAL DYNAMICS | CONVAIR

FOREWORD

This report presents the results of a study to determine the stability properties of the Centaur stage propellant utilization control system. This study was performed under Contract NAS3-3232.

Prepared by W. O. Stubblefield
W. O. Stubblefield
Senior Dynamics Engineer

Checked by R. F. Ringland
R. F. Ringland
Design Specialist

Approved by D. R. Lukens
D. R. Lukens
Dynamics Group Engineer

Approved by R. E. Martin
R. E. Martin
Chief of Dynamics

Approved by R P Dey for
H. L. Newman
Assistant Chief Engineer
Guidance and Control

SUMMARY

A propellant utilization control system is required to enable the Centaur vehicle to meet performance requirements. The system measures the mass of the propellants and controls propellant flow to the engines to keep the ratio between the propellant masses constant.

The stability qualities and closed-loop frequency response of the system were determined from the linearized equations describing the propellant-flow, propellant-sensor, and thrust-controller dynamics. The limit cycle characteristics were obtained by simplified phase plane analysis and an analog simulation, using all known system nonlinearities. The analog simulation was also used to determine the effect of propellant sloshing on system operation.

The results of these studies showed that the propellant utilization control system is stable using present gains with a possibility of a low-amplitude limit cycle. This limit cycle should have no appreciable effect on the overall system operation. The system behavior is essentially first-order, having a step response with a time constant of 6 seconds for small error signals. Since the expected changes in propellant ratio take place slowly, the only effect the low system gain will have is to increase the error in propellant ratio required to balance out an error in the trim mixture ratio of the engines.

The propellant utilization control system will operate in the presence of propellant sloshing of a magnitude to saturate the input to the servoamplifier. However, there will be a small steady-state error in the propellant ratio whose magnitude will depend on the amplitude and frequency of the propellant sloshing, the load on the electromechanical servo, and oxidizer-valve/engine-flow-rate gain. In addition to this steady-state error in the propellant mass ratio, there will be time-dependent errors that are functions of the servo positioner backlash, the loading and feedback gain, and the propellant slosh amplitude and frequency. Note that this study does not include an analysis of system errors on the ability of the Centaur vehicle to meet performance requirements.

TABLE OF CONTENTS

TABLE OF CONTENTS, Contd

LIST OF ILLUSTRATIONS

LIST OF ILLUSTRATIONS, Contd

LIST OF TABLES

LIST OF SYMBOLS

Symbol	Definition	Units
K	Velocity gain	deg/sec/volt
K_A	Summing bridge-amplifier gain	volts/lb
K_F	Fuel flow rate gain	lb/sec/deg
K_I	Acceleration gain	deg/sec^2/in.-lb
K_N	Servomotor velocity feedback gain	in.-lb/deg/sec
K_O	Oxidizer flow rate gain	lb/sec/deg
K_P	Valve stop spring constant	in.-lb/deg
K_S	Servoamplifier gain	volt/volt
K_T	No-load stall torque gain	in.-lb/volt
K_V	Oxidizer valve position to give 9-percent change in mixture ratio	deg
K_θ	Position feedback gain	volts/deg
$K_{\dot{\theta}}$	Viscous friction coefficient	in.-lb/deg/sec
L	Lagrangian function	ft-lb
Q_i	Forces not arising from a potential	lb
q_i	Generalized coordinates	N.D.
T	Kinetic energy	ft-lb
V	Potential energy	ft-lb
W_{OE}	Equivalent oxidizer	lb
$\dot{W}_{OE}$	Equivalent oxidizer flow rate	lb/sec

LIST OF SYMBOLS, Contd

Symbol	Definition	Units
W_F	Fuel weight	lb
$\dot{W}_F$	Fuel flow rate	lb/sec
W_O	Oxidizer weight	lb
$\dot{W}_O$	Oxidizer flow rate	lb/sec
α_T	Axial acceleration	ft/sec^2
ζ_F	Fuel probe damping	N.D.
ζ_O	Oxidizer probe damping	N.D.
θ	Oxidizer valve position	deg
θ_b	Backlash oxidizer valve shaft to feedback potentiometer	deg
θ_E	Servomotor input voltage	volts
θ_F	Oxidizer valve feedback position	deg
ρ	Density	$slugs/ft^3$
$\tau(K)$	Servomotor velocity time constant	sec
ω_F	Natural frequency, fuel probe	rad/sec
ω_O	Natural frequency, oxidizer probe	rad/sec
$f\left(\frac{\dot{\theta}}{\lvert\dot{\theta}\rvert}\right)$	Valve shaft load and friction	in.-lb

Mathematical Operators

Δ	Denotes perturbation
$\dot{}$ (dot)	Denotes differentiation with respect to time

SECTION 1

INTRODUCTION

This report presents the control dynamics analysis of the propellant utilization control system designed for the Centaur space vehicle. It is concerned with the stability and response properties of the control system within its expected operating range and environment. It does not include an analysis of the effect of system errors on the ability of the vehicle to meet performance requirements.

1.1 PURPOSE OF SYSTEM. The propellant utilization control system is intended to enable the Centaur vehicle to obtain the maximum amount of energy from given quantity of propellant. The system attains this end by measuring the ratio of the masses of the fuel and oxidizer and controlling their consumption rate to keep this ratio constant. The ability to keep the mass ratio constant depends on the accuracy with which the masses of the propellants can be measured and the capability of the propellant utilization control system to correct an indicated error in the relative masses of the fuel and oxidizer. Ideally this error should be zero throughout flight, but most importantly, at the end of flight if the maximum performance capabilities of the Centaur vehicle are to be realized.

1.2 SYSTEM DESCRIPTION. The propellant utilization control system measures the masses of oxidizer and fuel contained in the propellant tanks and controls the oxidizer flow by means of an electromechanical servo controlling a valve in the oxidizer line. The net result is a change in the mixture ratio of the propellants. Figure 1-1 is a pictorial diagram of the system.

The masses of fuel and oxidizer are measured by means of a capacitance probe in each tank. These probes consist of tubes with internal mandrels. The mandrel and the tube form the two plates of a capacitor whose value is dependent upon the radial separation distance between the mandrel and the tube and the dielectric constant of the medium between -- here, liquid or gas. As the fluid level drops, the dielectric constant changes, altering the capacitance. By properly tailoring the relative diameters of the mandrel and the tube, the capacitance can be made proportional to the mass of fluid in the tank. This capacitance is measured using a capacitance bridge. The ability of this type of probe to measure the mass of cryogenic propellant is discussed in Reference 1.

An error signal is generated by summing the difference between the oxidizer and fuel signals after the fuel signal has been amplified by a factor of five (the nominal mixture ratio). Thus an error of 5 pounds of oxidizer would be equivalent to 1 pound of fuel. The error signal is fed to a pair of electromechanical servos that position valves in the oxidizer feed lines, thereby changing the oxidizer flow rate. The thrust controller on each engine senses the change in thrust caused by the change in

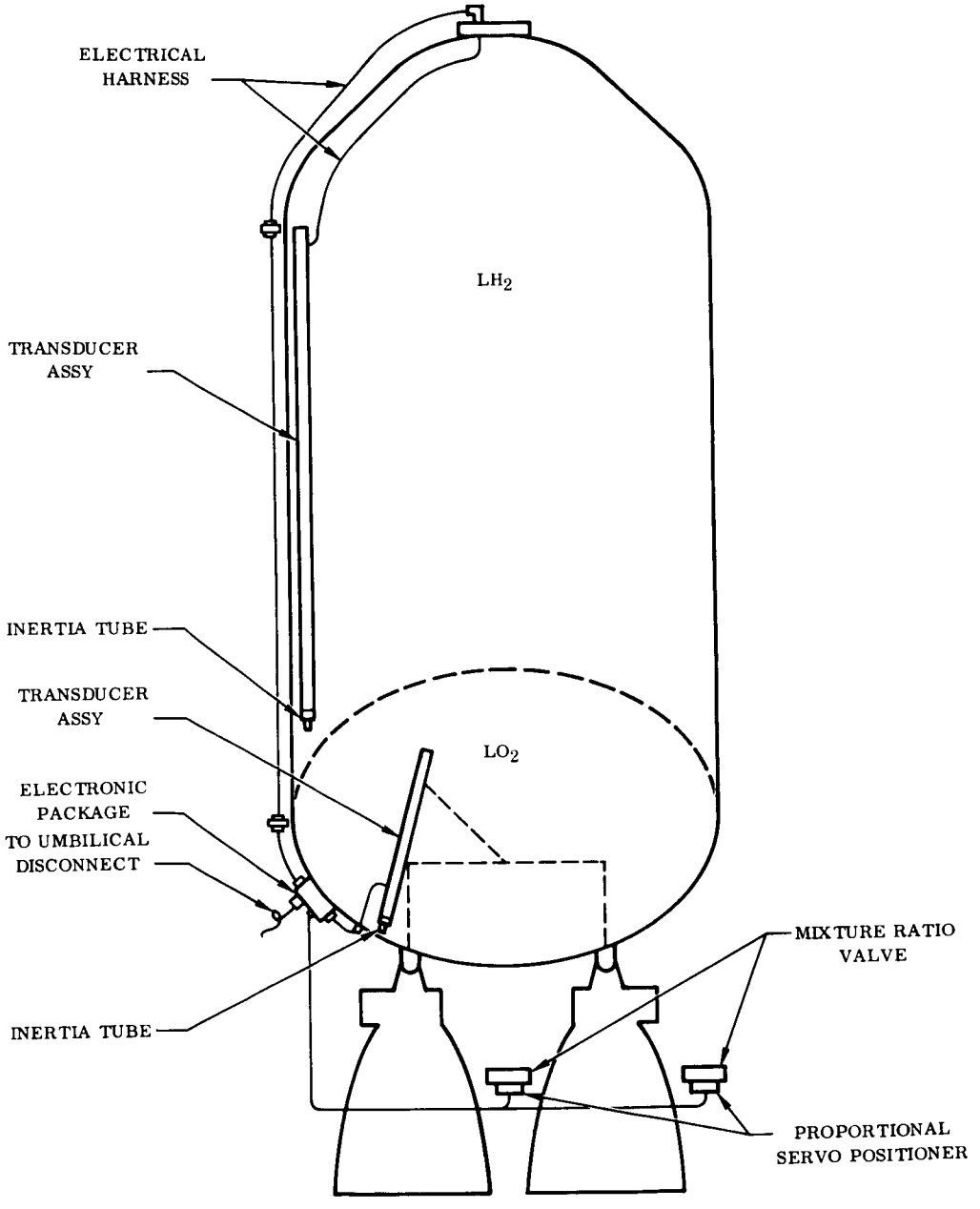

Figure 1-1. Propellant Utilization Control System Pictorial Diagram

oxidizer flow and changes the propellant pump speed, which in turn changes the fuel and oxidizer flow rates, to keep the thrust at a fixed level. The net result is a change in mixture ratio.

The electromechanical servo system has a two-phase motor to drive the pinion on the oxidizer valve through a 3200:1 gear train. Another parallel gear train is used to drive the position feedback potentiometer. The valve position depends on the error signal and the gain of the feedback signal. The maximum valve angle is determined by a pair of stops on the output of the gear. The motor characteristics determine the maximum velocity of the valve for a given input signal.

SECTION 2

LINEAR ANALYSIS

A mathematical model of the propellant utilization control system was derived in terms of the transfer functions of the component parts of the system about a nominal operating point. The stability of the linearized system was determined by solving for the root-loci of the resulting system of equations.

2.1 MATHEMATICAL MODEL. Figure 2-1 is a block diagram showing the relationship of the transfer functions. Both engines are assumed to have the same flow characteristics. Figure 2-2 shows the more general case where the two engines have different flow characteristics. Here, another parallel loop is added. The only differences in the two parallel loops are the K_θ, K_O, and K_F gains.

2.1.1 Propellant Flow Characteristics. The transfer function blocks for the engines, giving fuel and oxidizer flow as a function of the oxidizer valve position, were obtained from the engine manufacturer. (See Reference 2.)

2.1.2 Probe Characteristics. A derivation of the transfer functions for the propellant measurement probes is included in Appendix A.1. The probe characteristics vary as a function of the vehicle axial acceleration and the rate at which the propellant level is dropping in the tanks. In the fuel tank, this velocity is constant until late in the flight while in the oxidizer tank, it is continually changing due to the tank's ellipsoidal shape. The probe frequencies were calculated for several propellant levels and corresponding vehicle axial accelerations. The damping coefficients were determined from the slope of the head loss versus velocity loss curves shown in Figure 2-3. The curves, obtained from Reference 3, are given for an axial acceleration of 32.2 ft/sec^2 and are corrected for the accelerations used to calculate the probe frequencies. The accelerations and propellant masses are typical of the AC-7 mission and are taken from Reference 4. The results are applicable to other missions. The probe frequency is the most important parameter, since the damping does not vary a great deal with propellant level. For different payloads, the particular probe frequencies used in this study would occur at different flight times because of the difference in axial acceleration for a particular propellant mass. The depths to which the probes were immersed and the velocity of the fluid surface were calculated from data given in Reference 5.

2.1.3 Valve Position Servo. The electromechanical servo positioner is designed to move the oxidizer valve to give a specific change in oxidizer flow rate for each pound of equivalent oxidizer error due to an error in the ratio of propellants. Because of the servomotor characteristics, the gain, K, and the velocity time constant, $\tau(K)$, of the valve positioning system vary with the level of the valve angle error

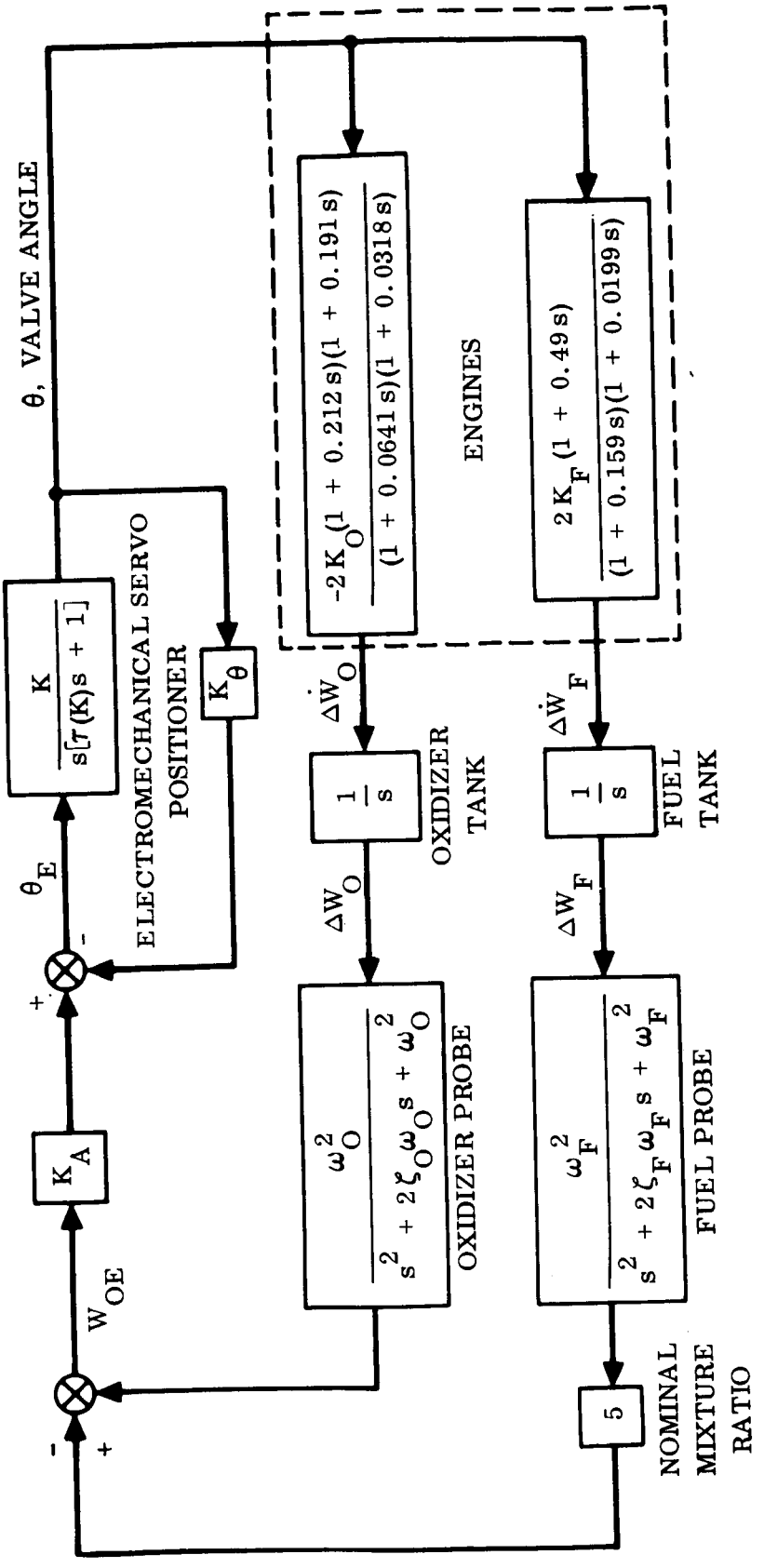

Figure 2-1. Simplified Block Diagram of Linearized Propellant Utilization Control System

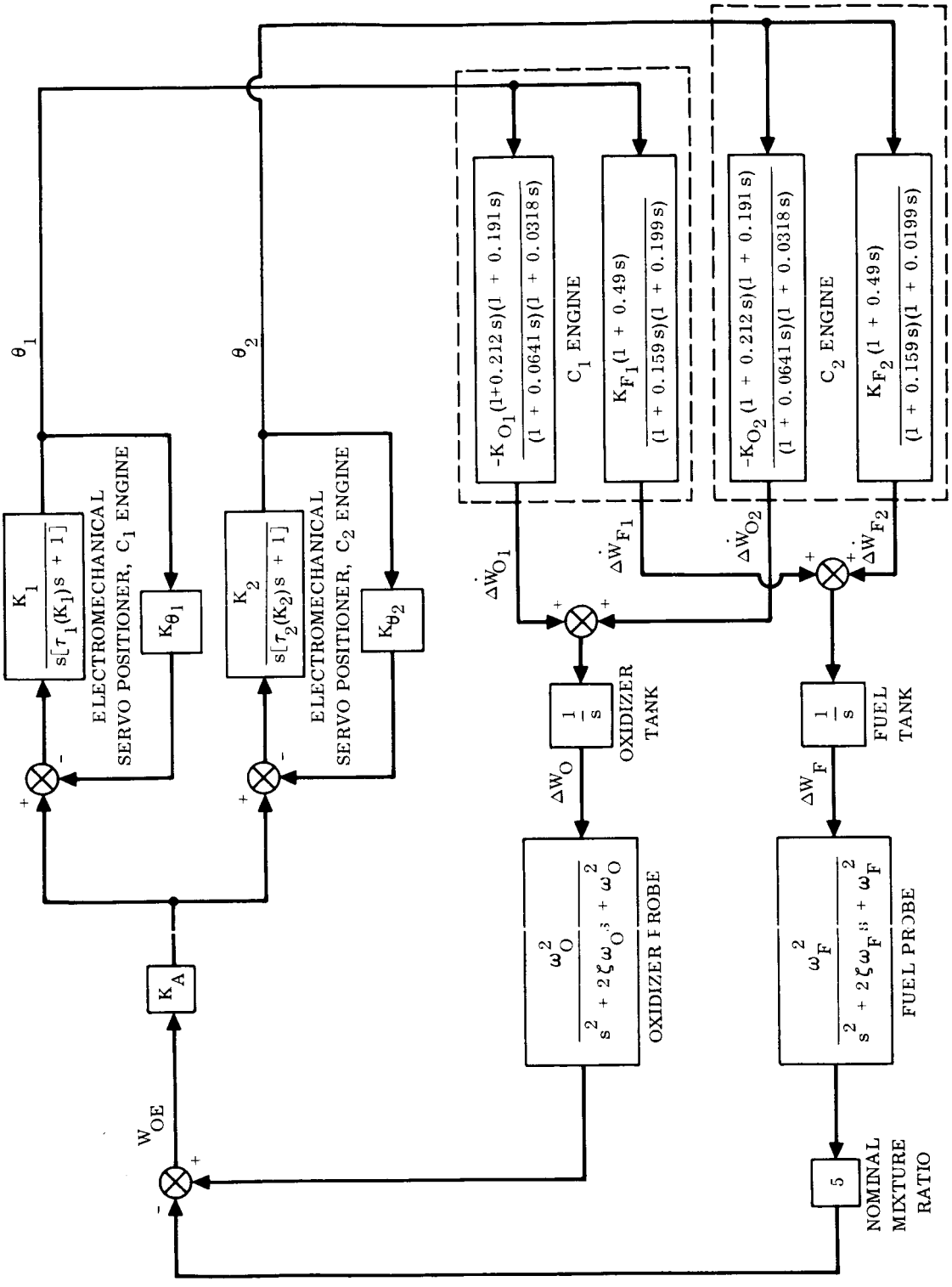

Figure 2-2. Block Diagram of Linearized Propellant Utilization Control System Showing Individual Engine Propellant Flow Characteristics

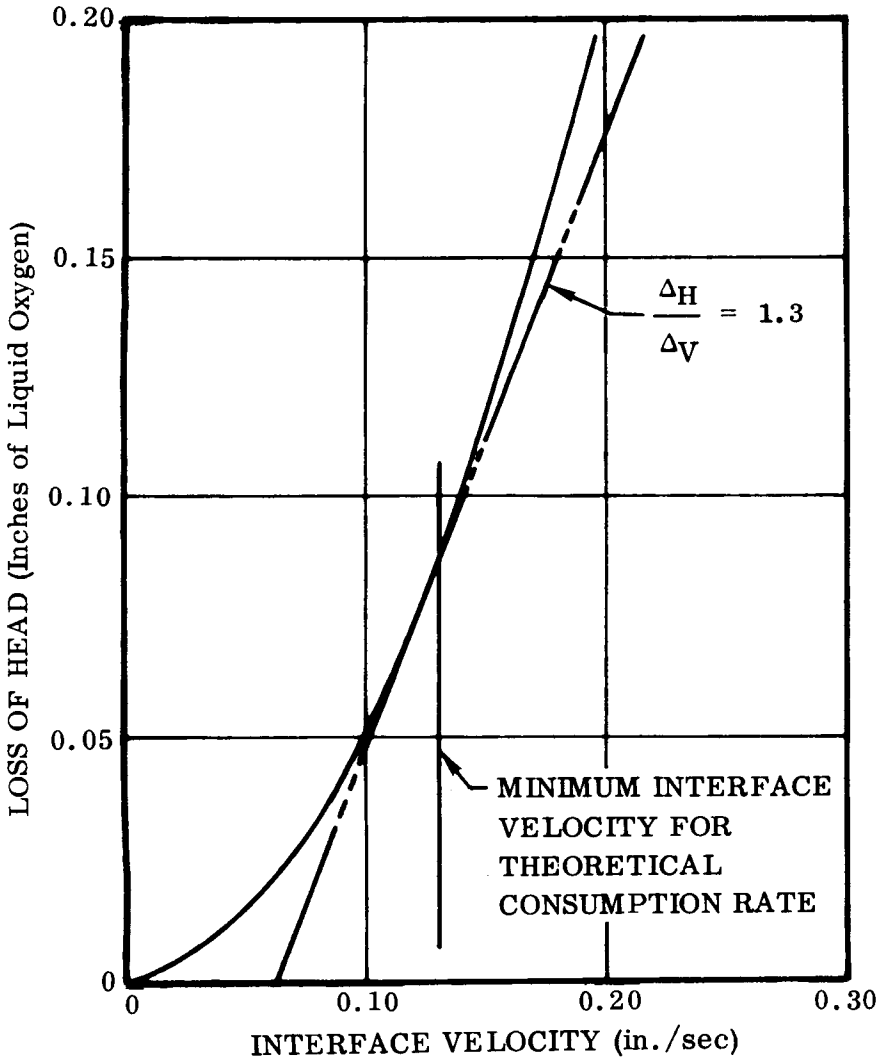

a. Relation Between Head Loss Lag and Interface Velocity for LO_2 Capacitance Probe Inertia Tube

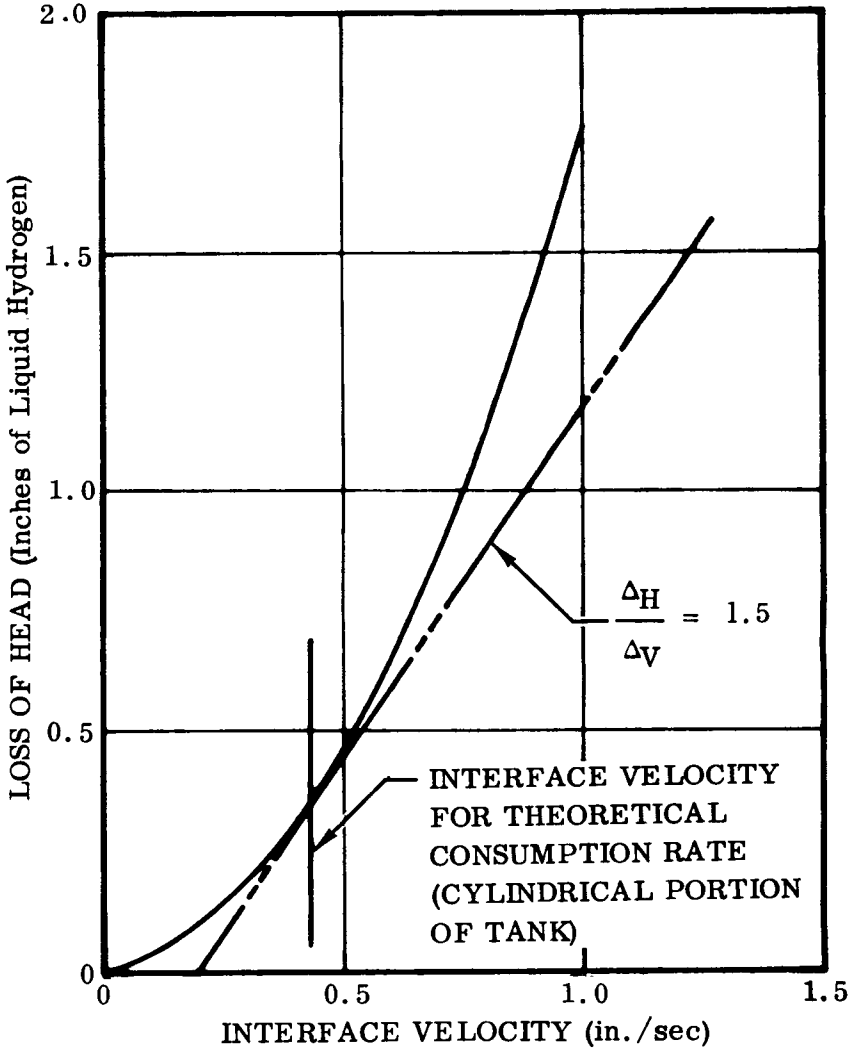

b. Relation Between Head Loss Lag and Interface Velocity for LH_2 Capacitance Probe Inertia Tube

Figure 2-3. Head Loss as a Function of Fluid Surface Velocity

signal (Figure 2-4). The method of determining the values used in the linear analysis is described in Appendix A.2.

2.2 ANALYTICAL RESULTS. The stability of the linearized system was studied at two times -- at the approximate midpoint and at the end of the propellant utilization control system's period of operation. The accelerations at these two times were taken as 54 and 91 ft/sec^2. The pertinent basic data are given in Appendix C. The root-loci of the propellant utilization control system were generated by varying the value of the summing bridge-amplifier gain, K_A.

2.2.1 Effect of Inertia Tubes. Originally, the capacitance probes were simple tubes with internal mandrels. With this system there is almost no damping for small changes in flow rate through the tubes. The root-loci for a propellant utilization control system using this probe system without compensation (Figure 2-5a) show that the system would be unstable for all values of K_A. The probes that are now used have a short inertia tube at the bottom of each probe. These tubes have a much smaller cross-sectional area than the probes. These restrictions provide damping and reduce the natural frequency of the probe/tank system. Figure 2-5b shows the root-loci of the control system with inertia tubes on the measurement probes for small amplitude error signals and nominal servo positioner feedback gain. At the nominal operating gains, ($K_A = 0.06$, $K = 35.2$, $K_\theta = 0.0735$), the system has a gain margin of 19 decibels.

2.2.2 Influence of Error Signal Magnitude. As stated in Section 2.1.3, the gain and velocity time constant of the valve positioning servo depend on the value of the valve position error signal. Root-loci for increasing values of error signal are shown in Figure 2-6. The major effect of an increasing error signal is to reduce the gain of the system at high frequencies. Figure 2-7 shows the closed-loop frequency response curves for large and small error signals. The system is linear for errors below 7.4 volts of valve position error voltage. As the error increases, the gain and velocity time constant decrease. At an error of 40 volts, the valve will be moving at its maximum rate. The valve will continue to move until it hits a stop set to give a change in mixture ratio of 9 percent. This is the maximum change that is presently allowed by engine operating considerations.

2.2.3 Influence of Valve Position Feedback Gain. The change in flow rate for a given change in valve position is not the same for all engines. To permit the calibration of each engine and electromechanical servo system so that the change in oxidizer flow rate per pound of equivalent oxidizer error is the same for all engines, the excitation voltage to the valve feedback potentiometer is changed by means of variable resistors connected to each one. This causes the valve to move a different number of degrees for the same error signal and results in the same overall outer loop gain at low frequencies. In Figure 2-1, the outer loop gain is $K_A(2K_O + 10K_F)/K_\theta$, and changes in K_O and K_F due to variations in engine characteristics may be

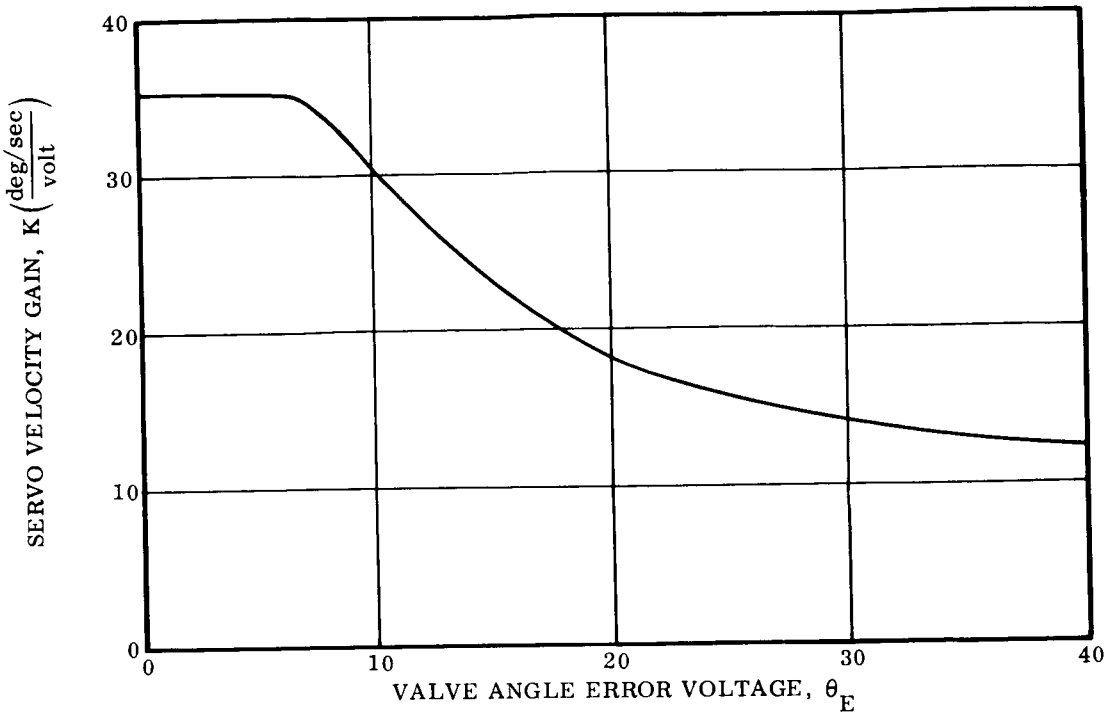

a. Velocity Gain

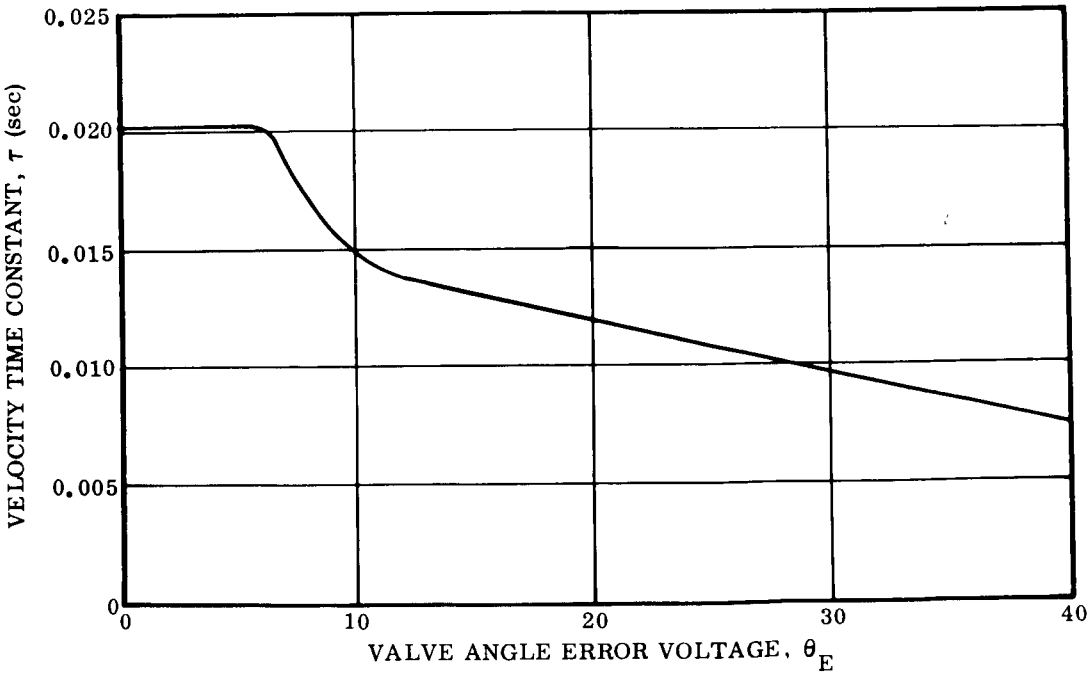

b. Time Constant

Figure 2-4. Valve Position Servo Characteristics

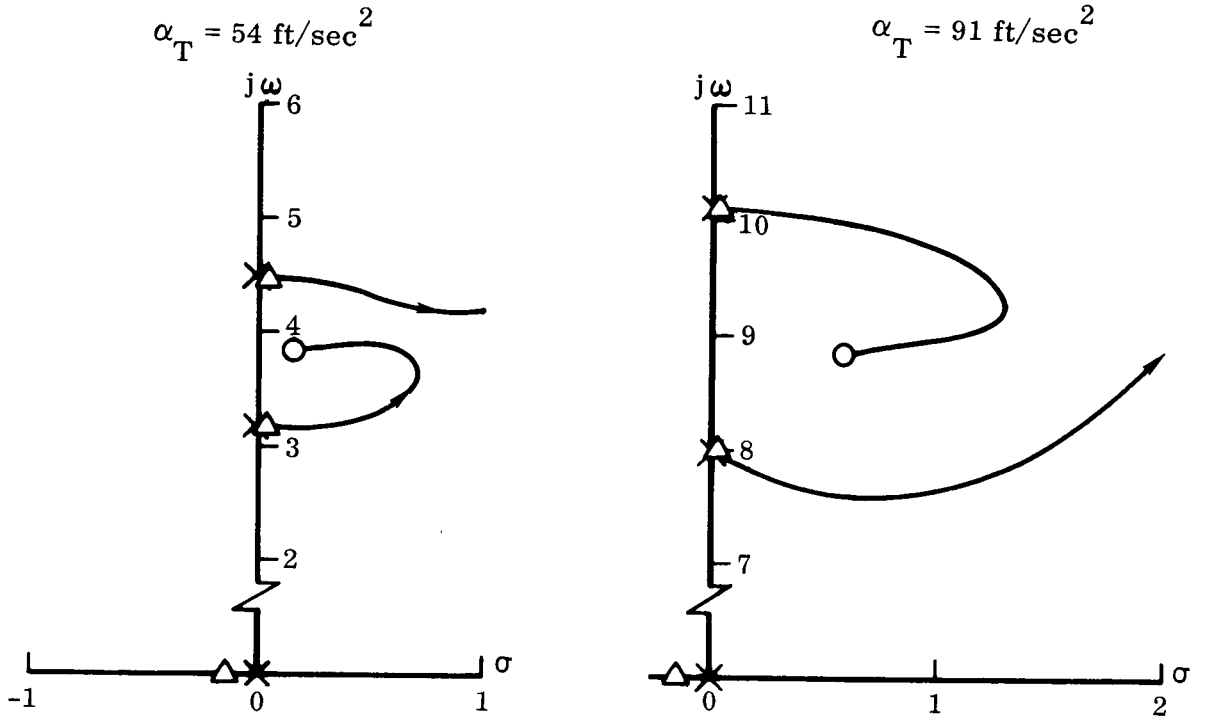

a. No Inertia Tube Compensation (Operating Point at Δ)

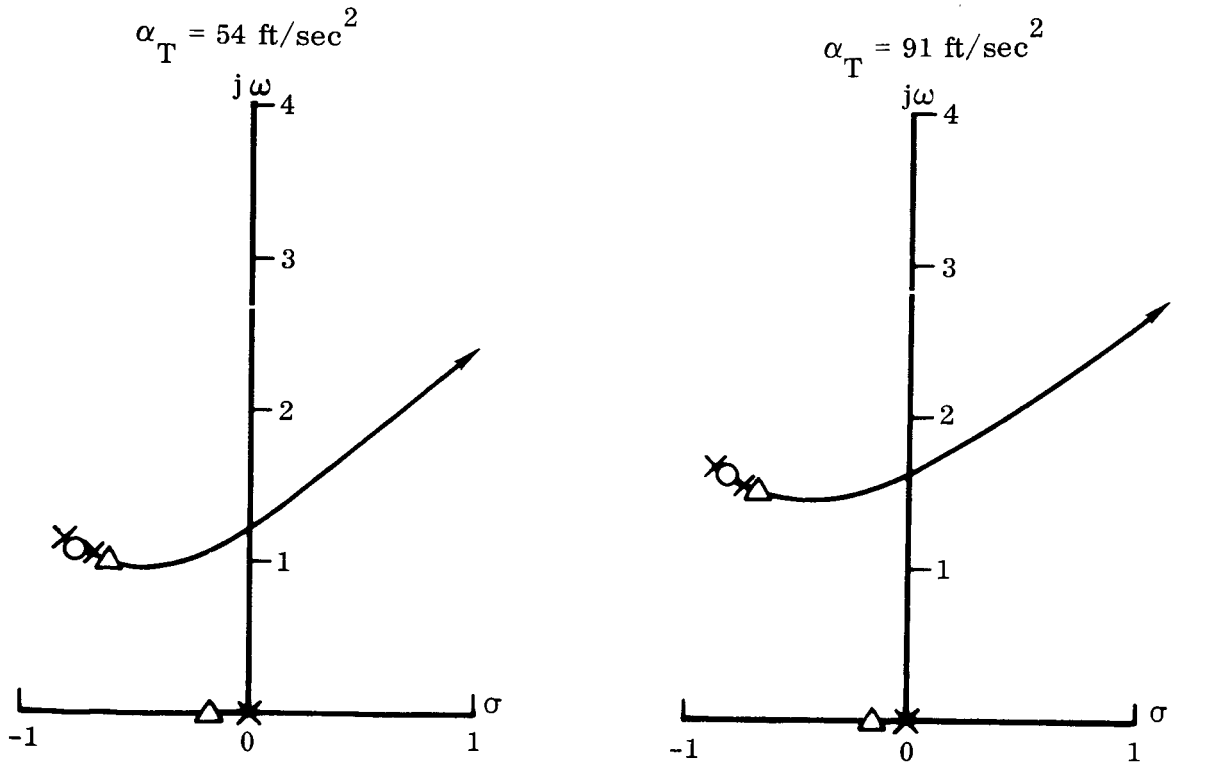

b. With Inertia Tube Compensation (Operating Point at Δ)

Figure 2-5. Linearized Stability With and Without Inertia Tubes, K_A = 0.06 volt/lb

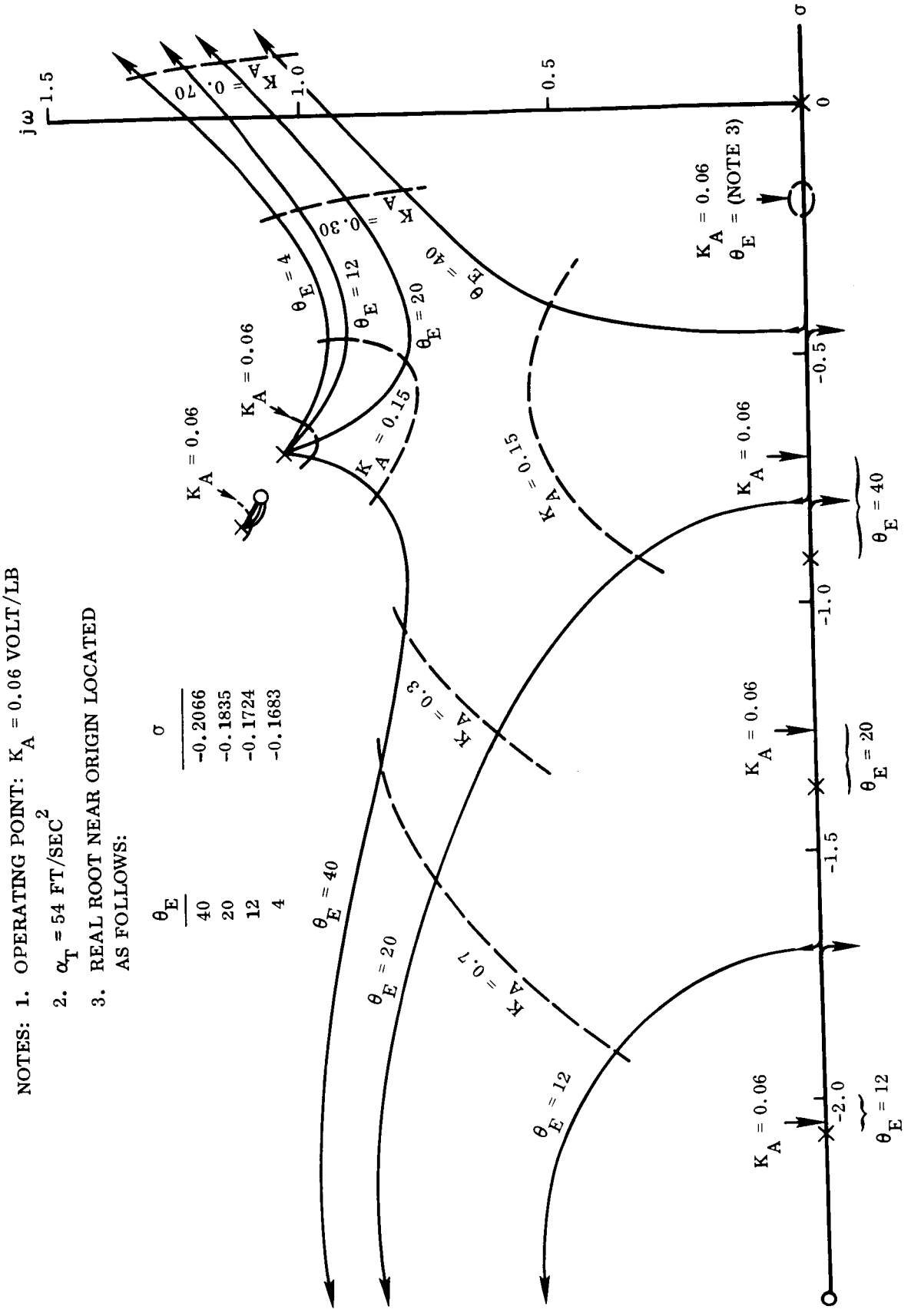

NOTES: 1. OPERATING POINT: $K_A = 0.06$ VOLT/LB

2. $\alpha_T = 54$ FT/SEC^2

3. REAL ROOT NEAR ORIGIN LOCATED AS FOLLOWS:

θ_E	σ
40	-0.2066
20	-0.1835
12	-0.1724
4	-0.1683

Figure 2-6. Stability With Varying Valve Position Error Voltage Levels

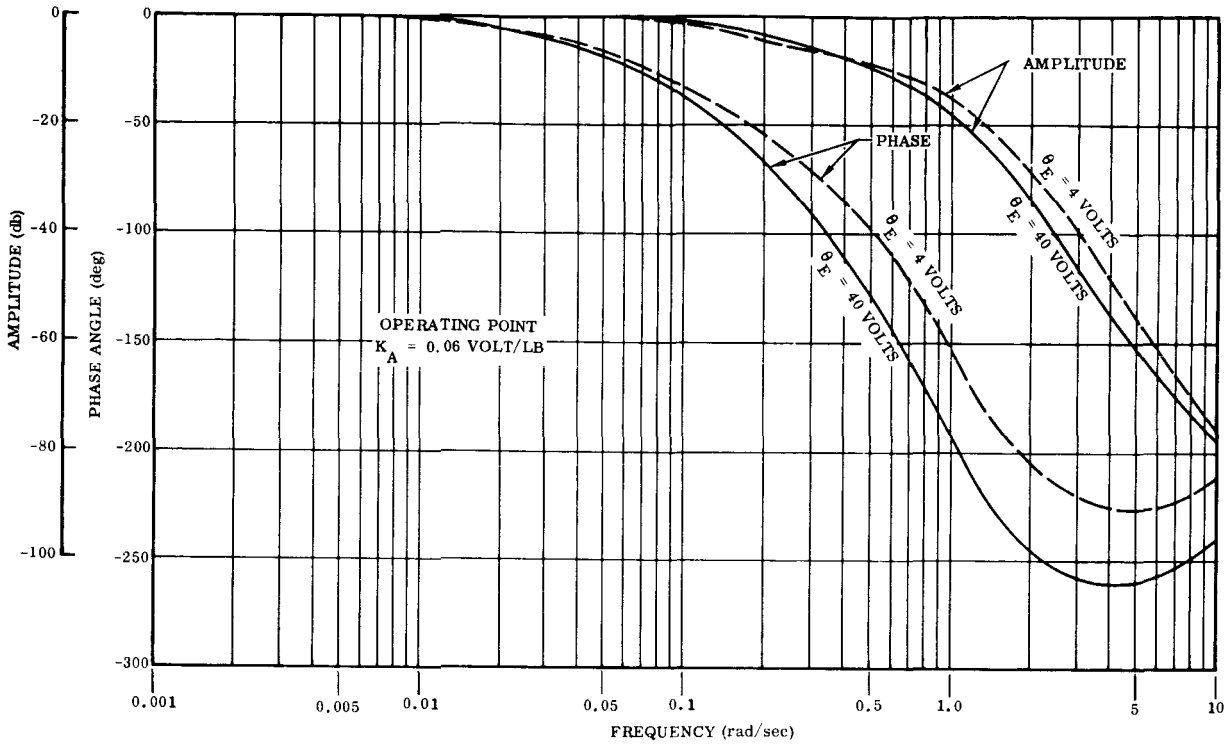

Figure 2-7. Frequency Response With High and Low Valve Position Error Voltage Levels

compensated for by corresponding changes in K_θ. However, the changes that result in the inner loop gain change the response of the servo positioner system. Figure 2-8 shows the effect on the root-loci of varying the feedback gain, K_θ, for accelerations of 54 and 91 ft/sec^2. Since the system gain is very low, the first critically damped root and the oscillatory roots do not change very much. The second over damped root changes appreciably, decreasing in frequency as the feedback gain is decreased. Due to the low system gain, the effect on system response is still not very great, as shown by the frequency response plots in Figure 2-9 for the highest and lowest values of K_θ used in Figure 2-8.

Since each engine can have a different oxidizer valve feedback gain, root-loci were plotted to determine the effect of one engine's having a high servo positioner feedback gain and the other engine's having a low one. Figure 2-10 shows the resulting root-loci. By comparing this figure with Figure 2-8a it is apparent that for the outer loop gain being used, system response will be almost the same as when both engines have a low feedback gain.

2.2.4 Influence of Asymmetric Thrust. Torques can be applied to the Centaur vehicle by operation of the propellant utilization control system. This can happen if a pair of engines do not have the same engine/valve gain. The maximum thrust

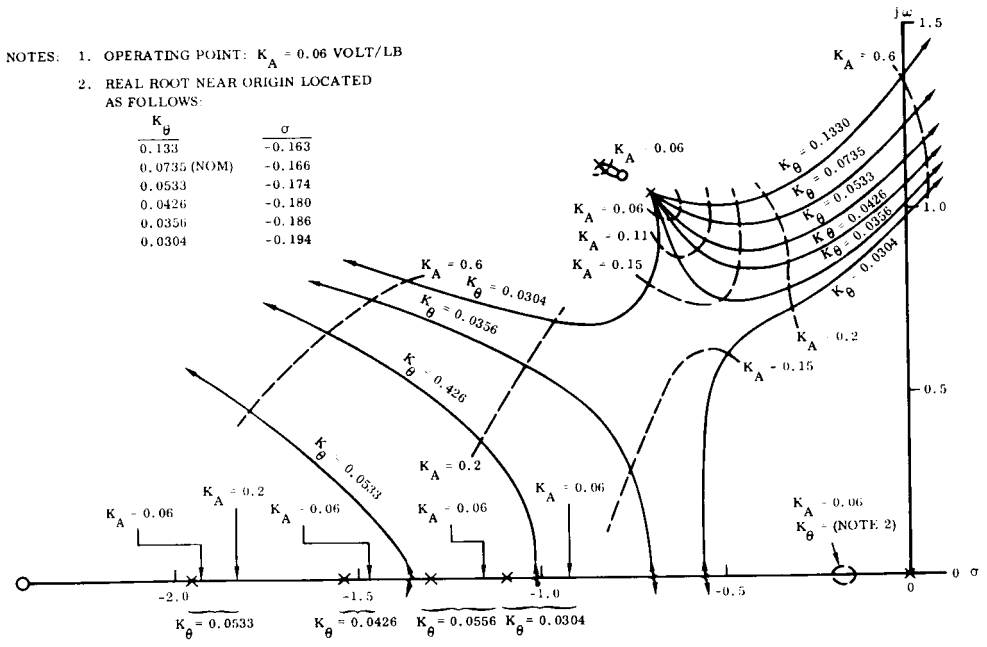

a. α_T = 54 ft/sec^2

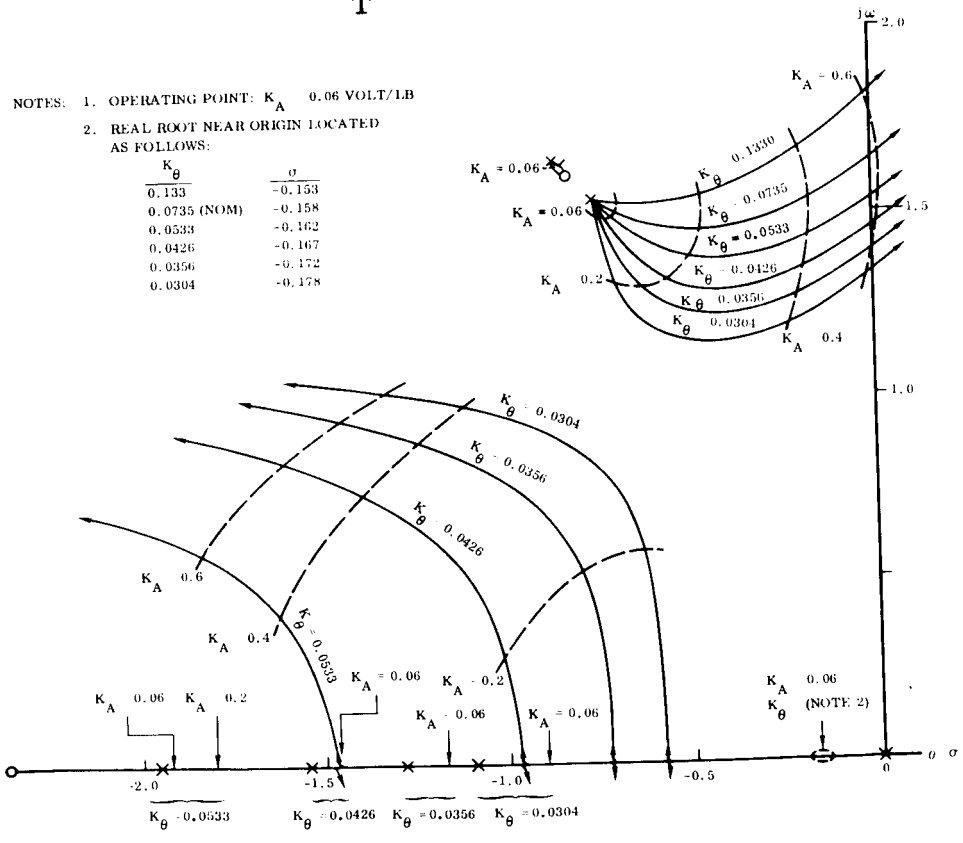

b. α_T = 91 ft/sec^2

Figure 2-8. Stability With Varying Valve Position Feedback Gain

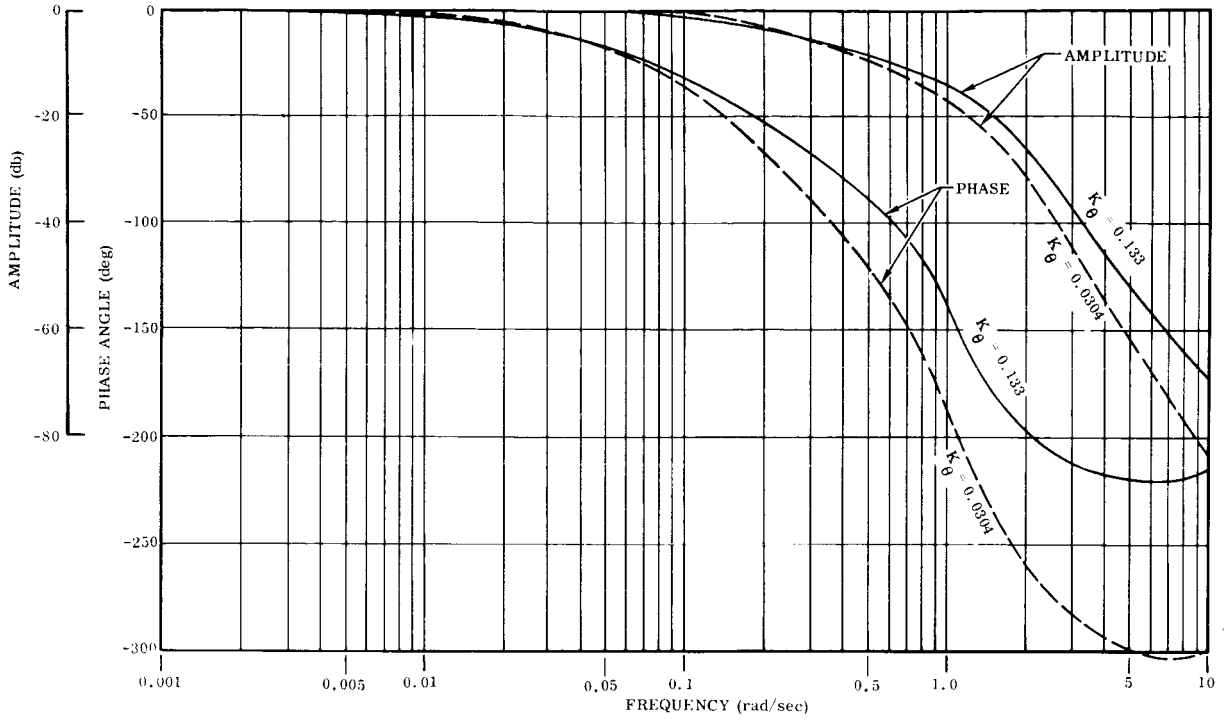

Figure 2-9. Frequency Response With High and Low Valve Position Feedback Gains

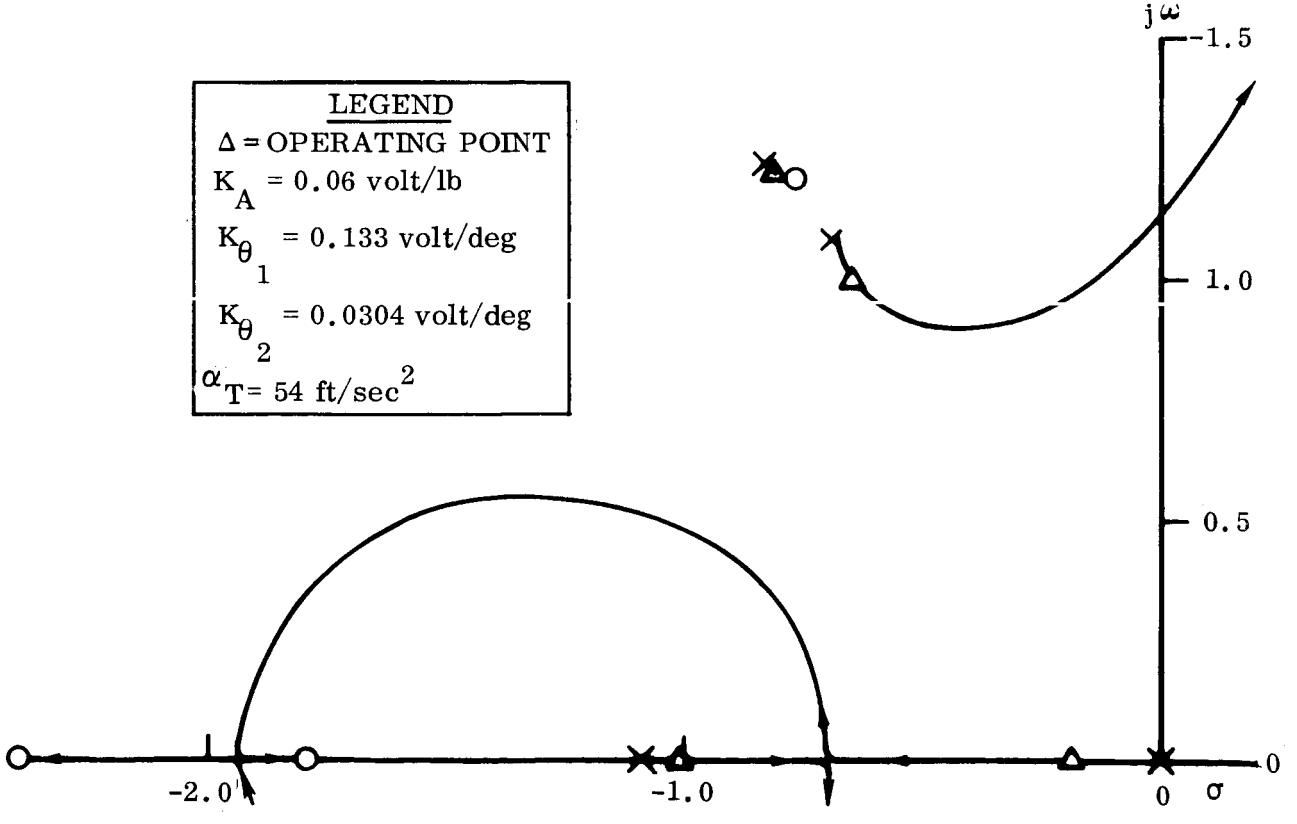

Figure 2-10. Stability With Different Valve Position Feedback Gains on Each Engine

differential of 91.5 pounds would take less than 0.1 degree of engine deflection to trim out. This is a transient value. The maximum rate of change is less than 0.04 deg/sec. This would only happen in response to step error in the ratio of propellants large enough to drive the valves to their stops and for K_V's of 15 degrees and 70 degrees for the engines. Since the engines can deflect 3 degrees, a transient due to the propellant utilization control system is insignificant. In addition the propellant-measuring probes are placed in a plane at right angles to the plane of the engines. Therefore, there will be no direct closed-loop coupling between the propellant utilization control system and the engines — engine motion in response to propellant utilization system commands produces fluid motion which cannot be sensed by the probes.

2.2.5 Additional Bias Errors. A steady-state error in the ratio of propellant masses can result if the engine is not operating at the correct mixture ratio when the oxidizer valve is in zero position. This can happen in several ways. First, when the valve and engine are calibrated, there is a tolerance on setting the mixture ratio. Second, the conditions of temperature and pressure that affect mixture ratio will not be the same as during calibration and will vary during flight. Reference 6 gives a random uncertainty of mixture ratio of ± 2.6 percent. To compensate for this error in mixture ratio would require a steady-state error of 10.3 pounds of equivalent oxidizer.

2.3 LINEAR STABILITY SUMMARY. The propellant utilization control system, as presently configured, is stable as a linear system and relatively insensitive to variations in either the magnitude of the error signal (mass ratio) or variations in the valve position feedback gain as used to compensate for variations in engine characteristics. This is indicated by the relatively small change in the closed-loop frequency response to error disturbances. This response is flat to approximately 0.06 rad/sec, having less than 25 degrees of phase lag at that frequency. Any significant peaking in the response is prevented by inertia tubes at the bottom of the capacitance probes. In addition, the system is relatively insensitive to changes in axial accelerations within the ranges to be encountered during a typical Centaur powered phase.

No coupling between the propellant utilization control system and the flight control system is possible because of the probe's location. Further, while action of the propellant utilization control system can cause a flight control system disturbance, the magnitude is insignificant.

SECTION 3

LIMIT CYCLE ANALYSIS

To study the effect of system nonlinearities on the stability of the propellant utilization control system, the transfer functions used in the linear analysis were simplified, and the effects of backlash in the gear trains between the motor shaft and the oxidizer valve and feedback potentiometer were added. Figure 3-1 is a block diagram of the simplified transfer functions.

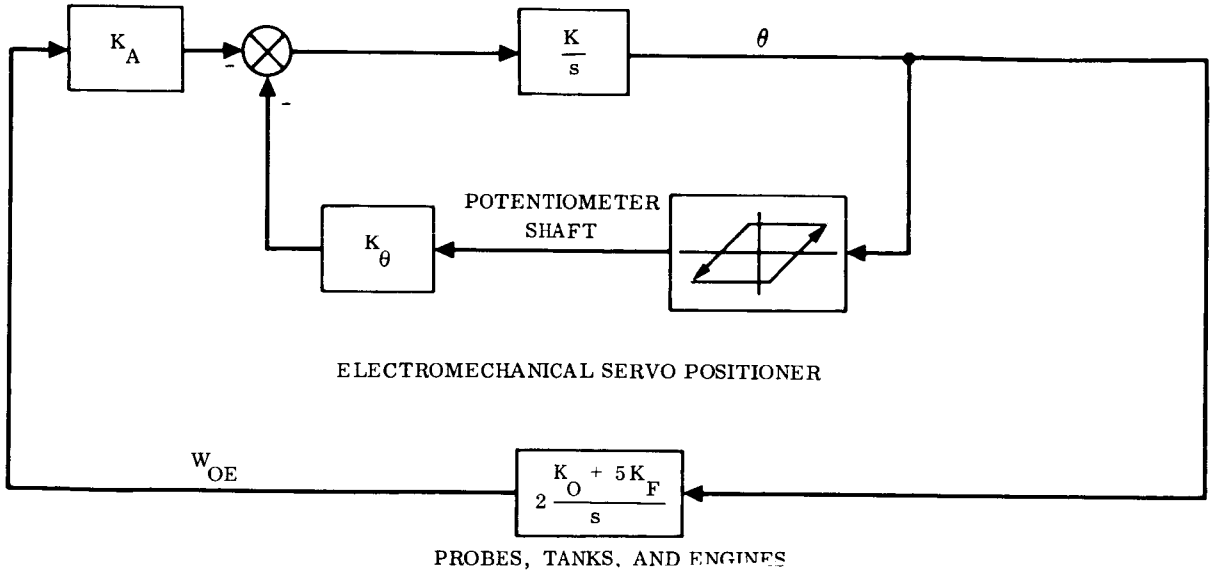

Figure 3-1. Block Diagram Used in Low-Frequency Limit Cycle Analysis

3.1 MATHEMATICAL MODEL. Separate gear trains connect the servomotor output to the feedback potentiometer and to the shaft operating the oxidizer valve. The specifications for the motor and gear train allow backlash to occur between the motor shaft, the valve operating shaft, and the feedback potentiometer shaft. Because of the way the gear train specifications are written, the allowable backlash between the motor shaft and the feedback potentiometer shaft is a function of the backlash between the motor shaft and the output shaft. The maximum backlash between the motor shaft and output shaft is 1/2 degree. The output shaft and the potentiometer

shaft are to be within ± 1 degree. For example, the backlash between the potentiometer shaft and the motor shaft can be only 1/2 degree when the backlash between the motor shaft and the output shaft is at its maximum of 1/2 degree.

The description of the mathematical model used for the analog simulation as well as the block diagram is given in Appendix B. In this model the limits on the system, the servomotor nonlinearities, the friction, and the loads as well as the gear train backlash were included.

3.2 ANALYTICAL RESULTS. For all possible dead bands between the motor shaft and the feedback potentiometer shaft, the valve positioning servo (inner loop) will be stable. There can be an error in valve position, its magnitude depending on the backlash between the valve shaft and the feedback potentiometer shaft. This will cause a limit cycle in the outer loop. (See Appendix A.3.) The amplitude and frequency depend on the amount of backlash, the load on the output of the gear train, and the gain of the outer loop. For a nominal K_V of 29 degrees, the maximum amplitude would be 2.95 pounds of equivalent oxidizer error with a period of 40.3 seconds. Figure 3-2 is a phase plane representation of this limit cycle. The limit cycle is not symmetrical because the load seen by the gear train is asymmetrical. The load used to obtain this limit cycle was 60 in.-lb for a positive valve deflection and 0 in.-lb for a negative valve deflection. Table 3-1 gives the calculated amplitudes and periods of the limit cycles for three values of K_V. For other combinations of loads, dead bands, and K_V, the periods will be shorter and the amplitudes smaller.

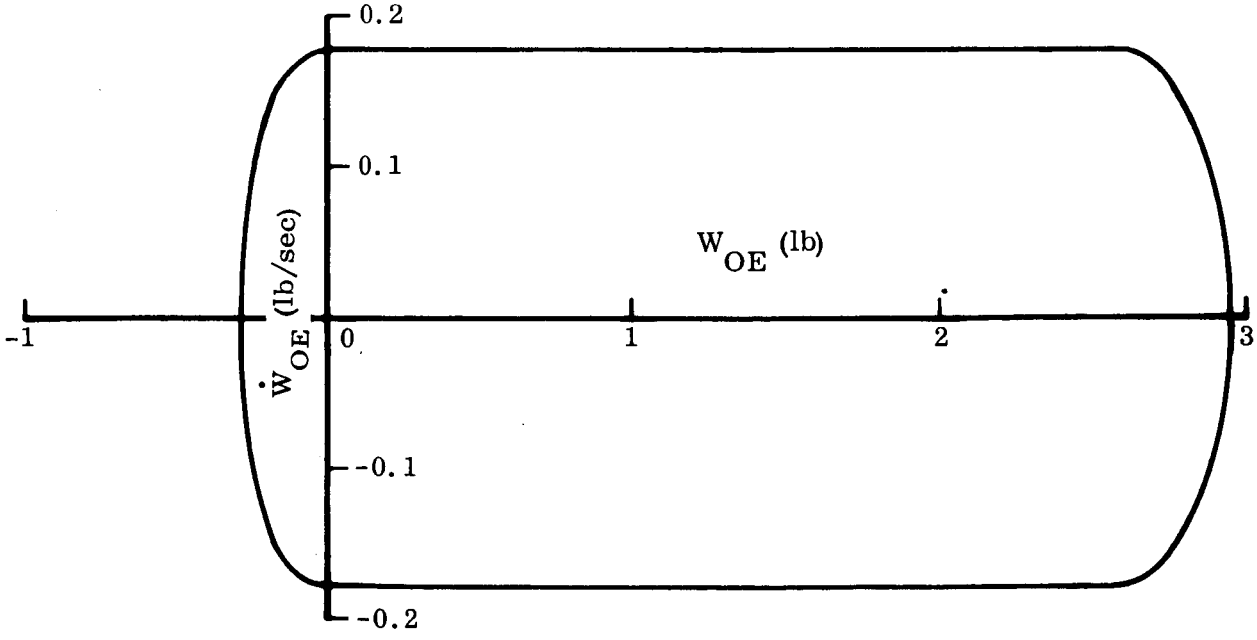

NOTES:
1. BACKLASH OXIDIZER VALVE SHAFT TO FEEDBACK POTENTIOMETER, ±1 DEG
2. BACKLASH OXIDIZER VALVE SHAFT TO MOTOR SHAFT, ZERO
3. OXIDIZER VALVE SHAFT LOAD, - 60 IN.-LB, ZERO

Figure 3-2. Analytical Limit Cycle Prediction, K_V = 29 degrees

Table 3-1. Limit Cycle Period and Amplitude, Calculated

K_V, VALVE ANGLE FOR 9-PERCENT CHANGE IN MIXTURE RATIO (degrees)	PERIOD OF LIMIT CYCLE (seconds)	MAXIMUM AMPLITUDE OF LIMIT CYCLE (pounds)
15	22.96	3.14
29	40.3	2.95
70	88.2	2.85

3.3 ANALOG SIMULATION RESULTS. The limit cycle characteristics of the system were confirmed by use of an analog simulation of the propellant utilization control system. Computer runs of the limit cycles resulting from a range of values for K_V are shown in Figures 3-3 through 3-6. These runs were made with the maximum expected asymmetrical load of 60 and 0 in.-lb. Figure 3-7 shows the limit cycle with a symmetrical load of 30 in.-lb. Table 3-2 is a listing of the amplitudes and periods for the three cases of Table 3-1.

Table 3-2. Limit Cycle Period and Amplitude, Analog Simulation

K_V, VALVE ANGLE FOR 9-PERCENT CHANGE IN MIXTURE RATIO (degrees)	PERIOD OF LIMIT CYCLE (seconds)	MAXIMUM AMPLITUDE OF LIMIT CYCLE (pounds)
15	19.5	3
29	34.5	2.8
70	72.5	2.75

3.4 CORRELATION BETWEEN ANALYTICAL AND ANALOG METHODS. Comparing Tables 3-1 and 3-2 it is clear that the amplitudes and periods for both the simple phase plane analysis and the analog simulation give almost the same results. The periods and amplitudes of the limit cycles obtained from the analog simulation are not as large as the calculated values. For example, the limit cycle period for the nominal valve/engine (K_V = 29 degrees) obtained from the analog simulation was 34.5 seconds while the phase plane calculation gave 40.3 seconds. The primary reason for this difference is that the phase lag and attenuation in the system due to the engine flow characteristics, the propellant probes, and the inertia of the servomotor and gear train were neglected in the phase plane calculation.

Because these lags reduce the error signal at a given time during a cycle, the backlash between the valve and feedback potentiometer is taken up. This has the effect of increasing the gain of the system, reducing the time required to change the increment in flow rate from positive to negative. The fact that the two methods give similar results supports the validity of using the phase plane method of calculating the limit cycle.

3.5 LIMIT CYCLE SUMMARY. The presence of backlash in the gear trains connecting the servomotor with the valve and the feedback potentiometer can lead to a low-amplitude (in terms of propellant mass ratio) limit cycle. This limit cycle is smaller than that which can result from calibration errors and far smaller than the allowable error of 150 pounds of equivalent oxidizer.

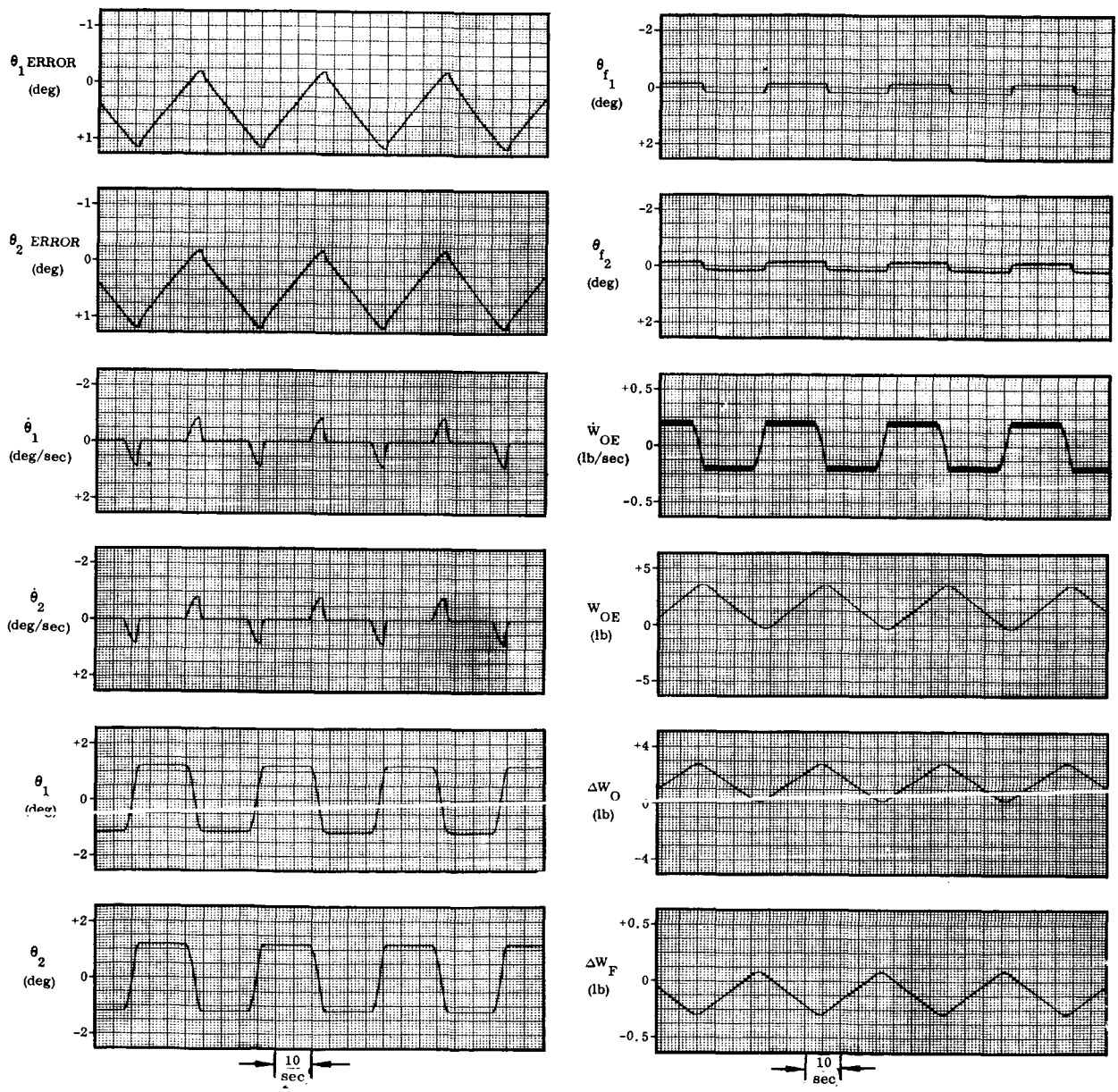

Figure 3-3. Limit Cycle Asymmetrical Load, K_V = 29 degrees

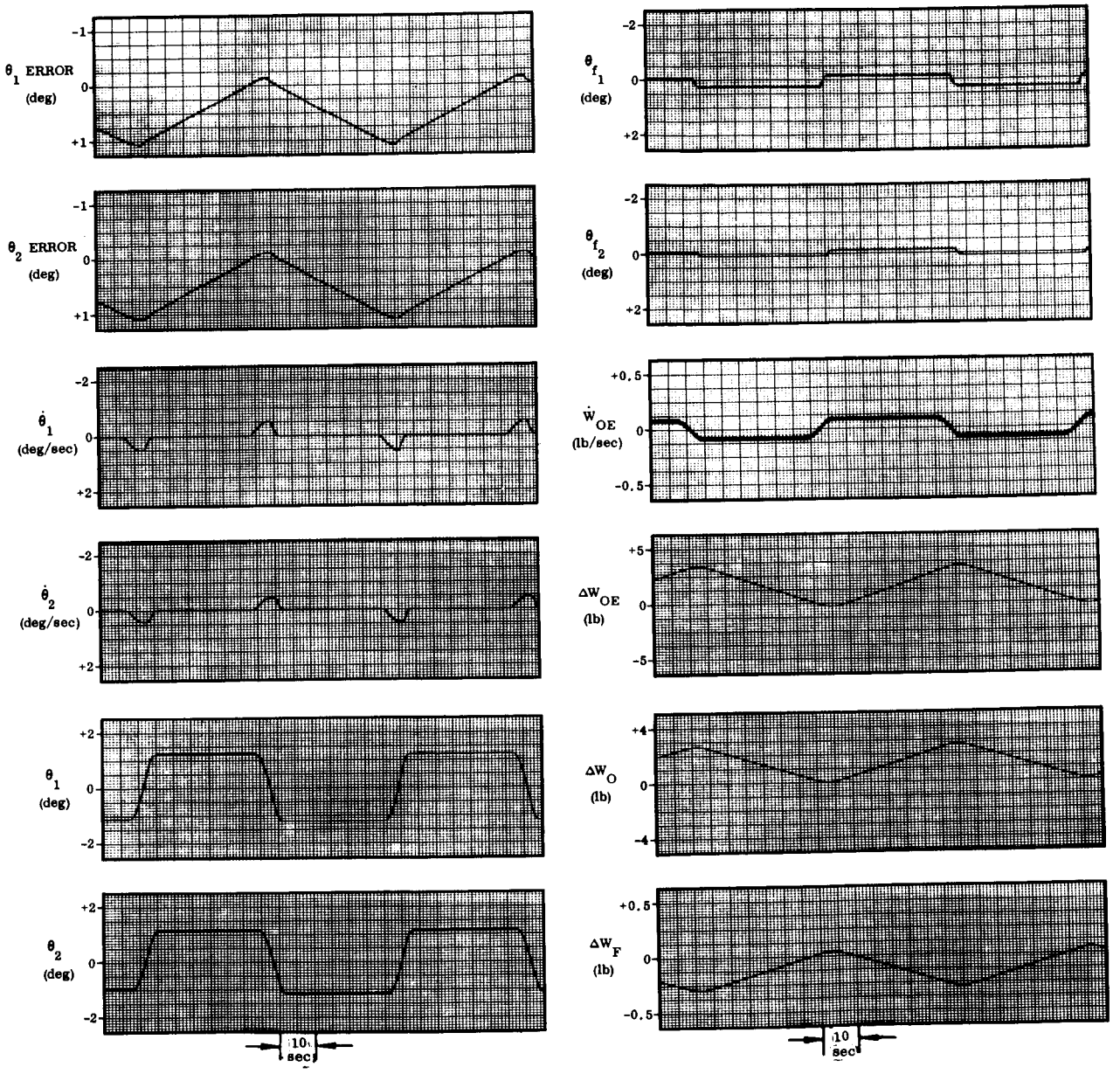

Figure 3-4. Limit Cycle Asymmetrical Load, K_V = 70 degrees

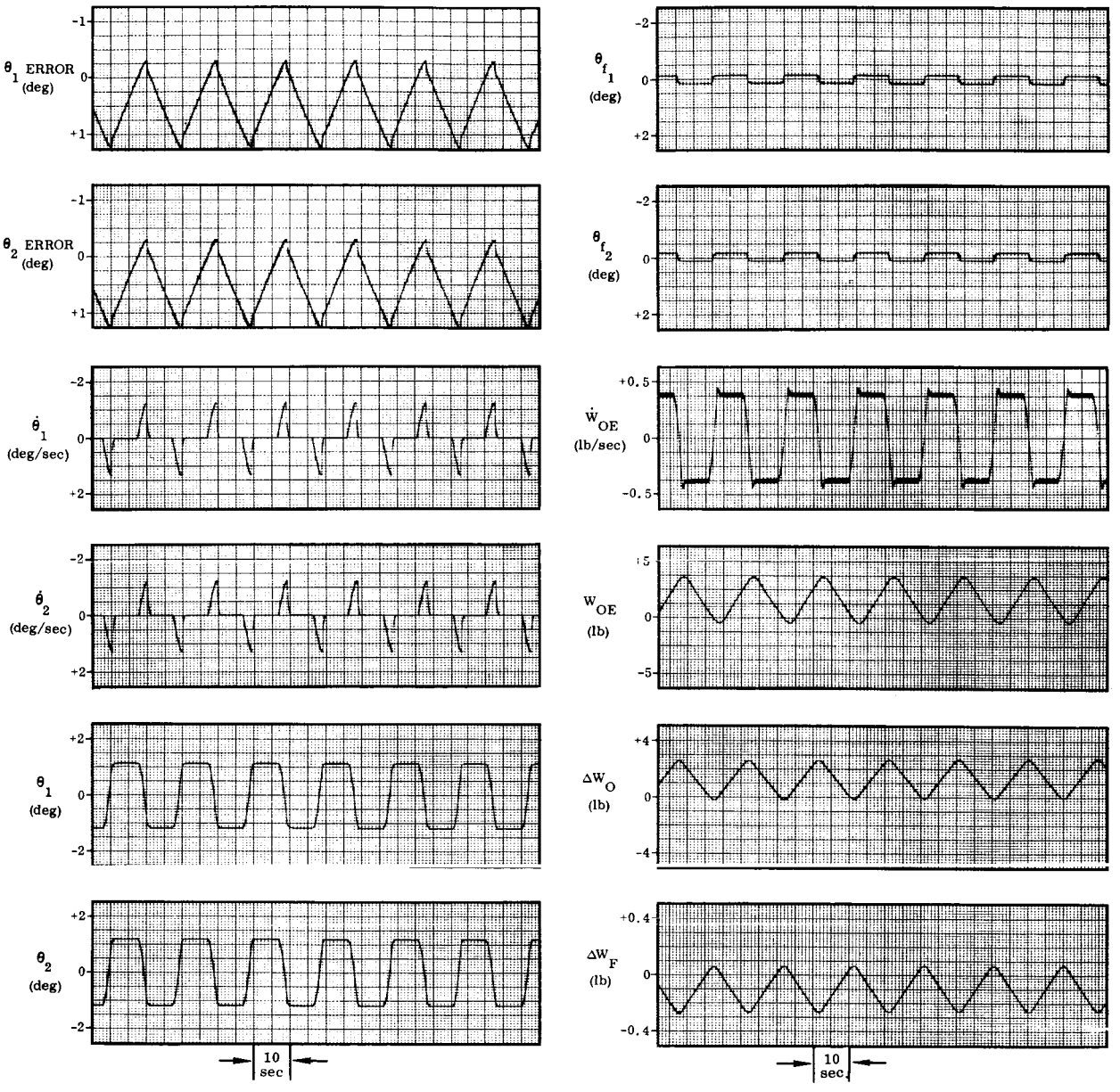

Figure 3-5. Limit Cycle Asymmetrical Load, K_V = 15 degrees

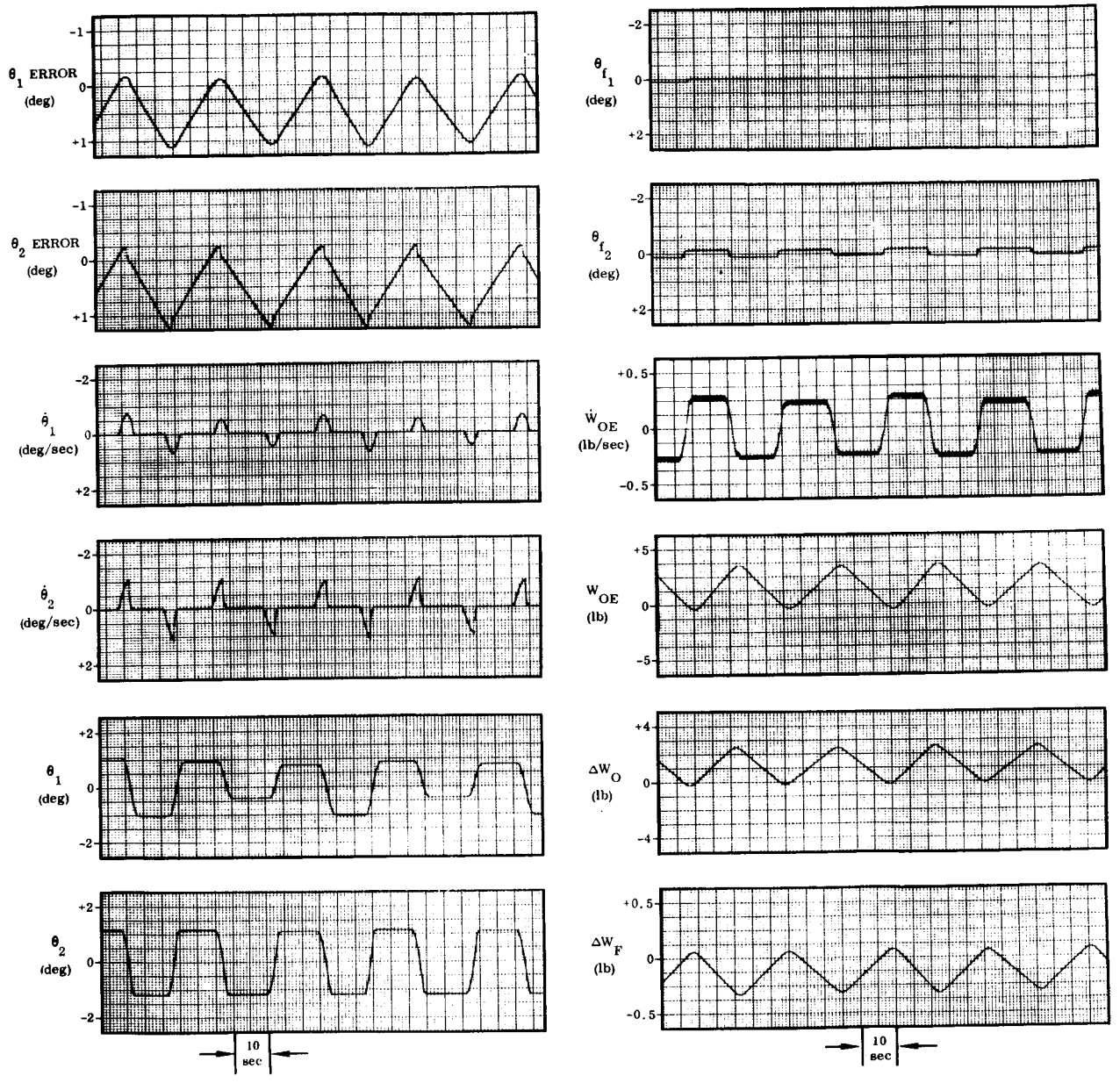

Figure 3-6. Limit Cycle Asymmetrical Load, θ_1 = 29 degrees, θ_2 = 15 degrees

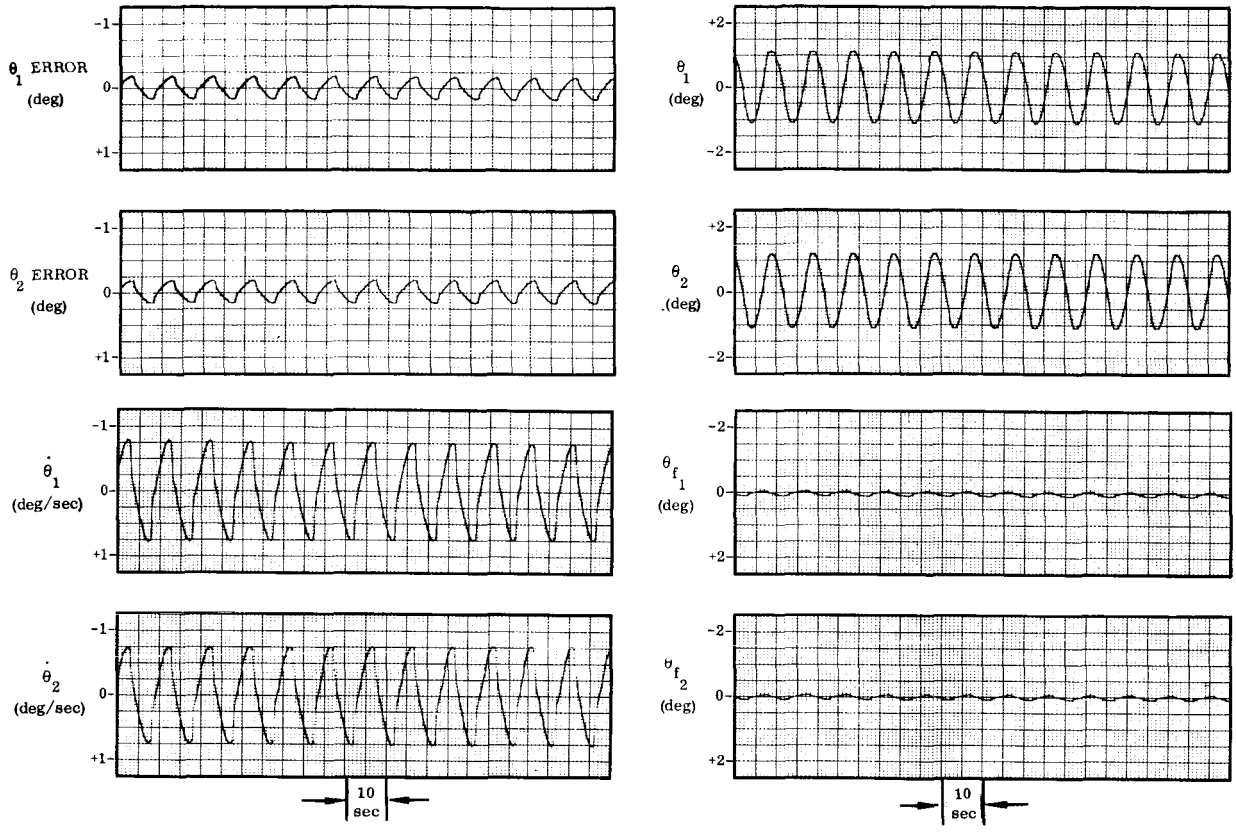

Figure 3-7. Limit Cycle Symmetrical Load, K_V = 29 degrees

SECTION 4

SYSTEM OPERATION IN THE PRESENCE OF PROPELLANT SLOSHING

A description and block diagram of the analog simulation used for the following analysis is contained in Appendix B.

4.1 STEP RESPONSE. Errors in the propellant ratio due to sloshing can saturate the input to the servoamplifier. The analog simulation of the propellant utilization control system was used to determine the ability of the system to correct for steady-state errors, not resulting from the dynamics of the control system, in the presence of this saturation. The system was set in operation with a 50-pound oxidizer error. The ability of the system to correct for this initial error is shown in Figures 4-1 through 4-3. One run is without propellant sloshing, and the others are for two different slosh frequencies. The response of the system is heavily dependent on the frequency of the sloshing. The step response with a sloshing frequency of 1 cps was almost identical to the step response with no slosh. The only difference was a small-amplitude ripple superimposed on the normal response. On the other hand, with 0.2-cps sloshing frequency, the response was underdamped compared with the other two cases. The time to reach a more or less steady-state condition was over five times as long as with 1-cps propellant sloshing.

4.2 RESPONSE TO PROPELLANT SLOSHING. Analog runs were made for a large range of sloshing and propellant utilization control system parameters. To give some idea of their effect on the steady-state operation of the system, several runs are included in Figures 4-4 through 4-15. The effects of sloshing are constant movement of the oxidizer valve and steady-state as well as time-dependent errors in the ratio of the propellant masses.

4.3 STEADY-STATE ERRORS DUE TO SLOSHING. The equivalent oxidizer error generated by propellant sloshing can cause a steady-state error in the ratio of the propellants. The reason for this error is that the error signal due to sloshing can be large enough to saturate the servomotor. Saturation will cause the servomotor to run at maximum velocity during each half of a cycle. This velocity will be higher in one direction than the other because of an asymmetrical load on the oxidizer valve. Since the time the valve is moving in each direction is about the same, the effective valve position will be such that oxidizer flow will increase. This increase will result in an error in the ratio of propellant masses. The mass error will generate a signal that will bias the valve position so that the average flow rates will be correct. The size of this error will depend on the frequency and amplitude of the sloshing, the position feedback gain, valve/engine flow rate gain, propellant measurement probe dynamics, and the load on the servomotor. The steady-state error is proportional to the asymmetrical load when all other parameters are fixed. To determine the effect of the other parameters, a series of runs was made, varying the sloshing

amplitude and frequency at two axial acceleration levels and three values of K_V. The two axial acceleration values gave a variation in probe dynamics. The three values of K_V gave variations in the feedback and valve/engine gains. Figure 4-16 plots the steady-state errors resulting from the runs.

The largest errors occur at low sloshing frequencies and high vehicle axial accelerations coupled with low position feedback and valve/engine gains. At excitation frequencies above 0.6 cps, the steady-state error does not increase very much with an increase in the sloshing amplitudes. The reason is that at low amplitudes, the normal asymmetrical limit cycle of the system predominates. The steady-state error due to the foregoing is almost equal to the steady-state error resulting from the propellant sloshing, which is dominant as its amplitude is increased.

4.4 TIME-DEPENDENT ERRORS DUE TO SLOSHING. In addition to the steady-state errors, there will be a time-varying error in the ratio of propellants. Curves showing the error amplitudes as a function of propellant sloshing frequency and amplitude are shown in Figure 4-17. The frequencies of the errors vary. These variations account for the curves not being smooth at all excitation frequencies. The errors will be at the sloshing frequencies, limit cycle frequencies, or combinations of both. The 0.6-cps curve in Figure 4-17a (54 ft/sec^2 value) is a good example for slosh amplitudes above 40 pounds. The error is the same as the sloshing frequency, and the curve is smooth. Below 40 pounds, the steady-state error is small enough to allow a limit cycle to start, and the limit cycle then becomes the dominant factor in determining the amplitude of the time-varying error.

4.5 SUMMARY OF SLOSHING INFLUENCE. The step response of the propellant utilization control system to a mass ratio error is rather slow, taking between 15 and 24 seconds for a transient to subside to a negligible level. The response time varies with changes in the error signal amplitude and the valve position feedback gain. For a step input, the overshoot is only 30 percent of the steady-state value -- indicating a well-damped system.

The system will operate satisfactorily in the presence of sloshing while still maintaining steady-state and time-dependent mass ratio errors within allowable limits. While sloshing heavily influences system behavior, resultant errors are small compared with those allowable. Moreover, the sloshing expected during those flight times when the system is in operation is rather small. (See Reference 7.)

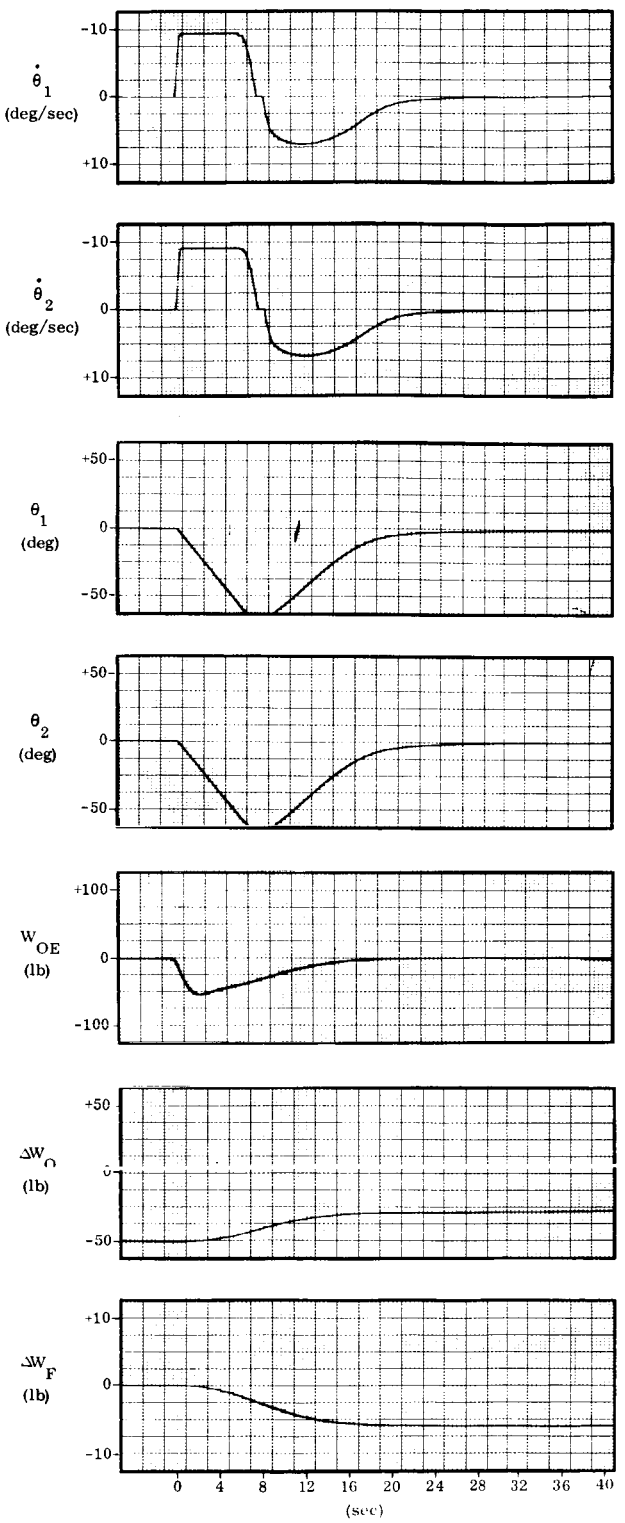

Figure 4-1. Step Response Without Propellant Sloshing, K_V = 70 degrees, α_T = 91 ft/sec^2

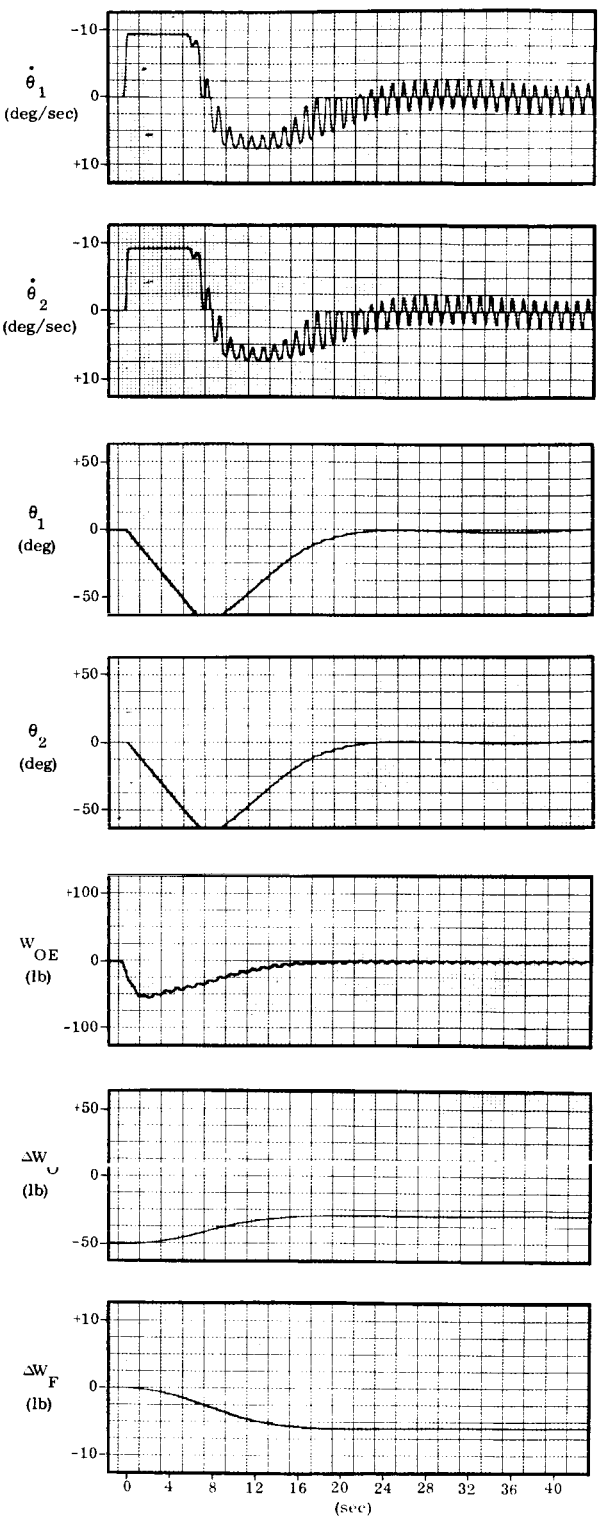

Figure 4-2. Step Response With Sloshing, f_{slosh} = 1 cps, K_V = 70 degrees, α_T = 91 ft/sec^2

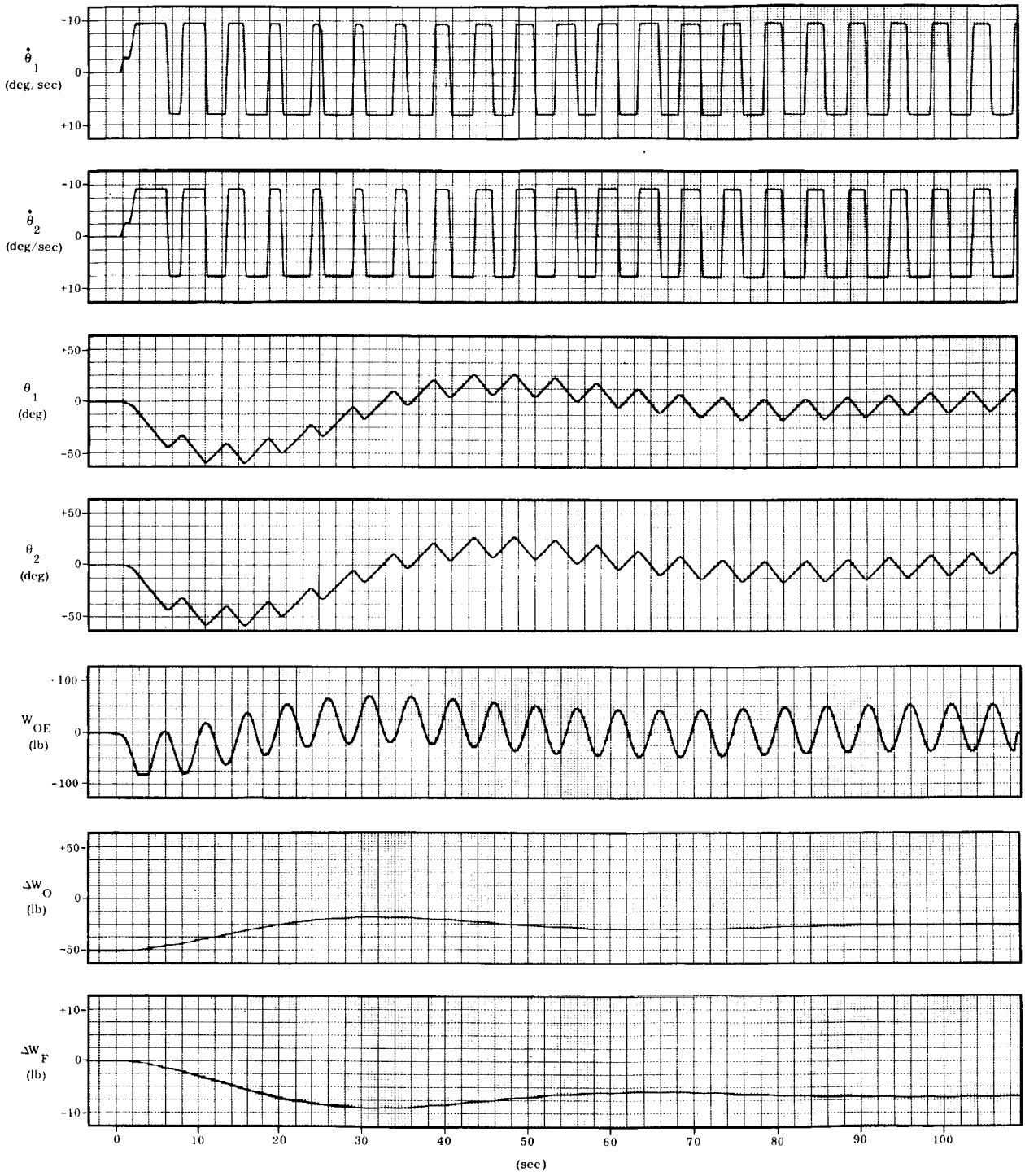

Figure 4-3. Step Response With Sloshing, f_{slosh} = 0.2 cps, K_V = 70 degrees, α_T = 91 ft/sec^2

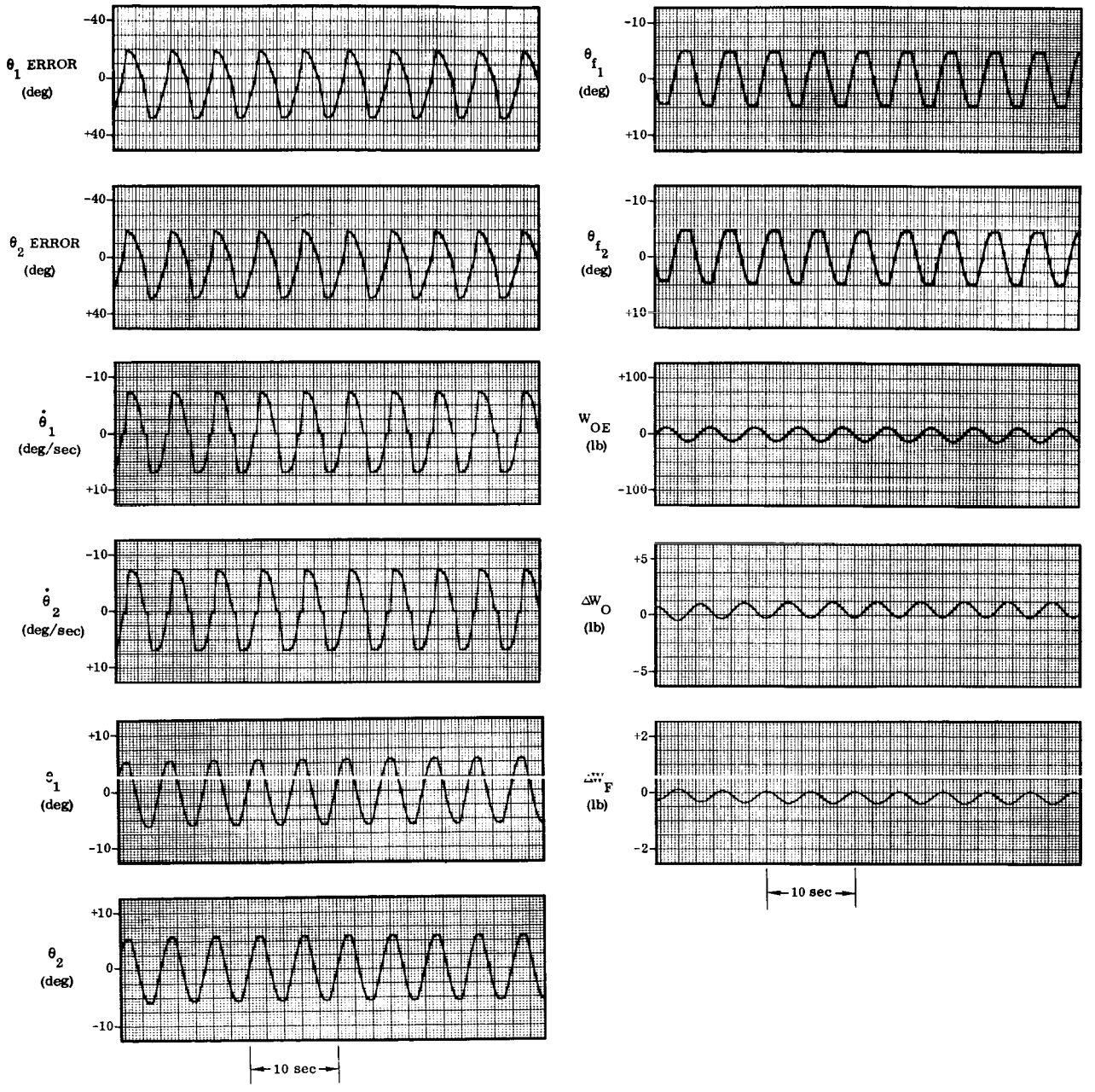

Figure 4-4. Slosh Response, Frequency = 0.2 cps, ΔW_O = 20 pounds peak-to-peak, K_V = 15 degrees, α_T = 91 ft/sec^2

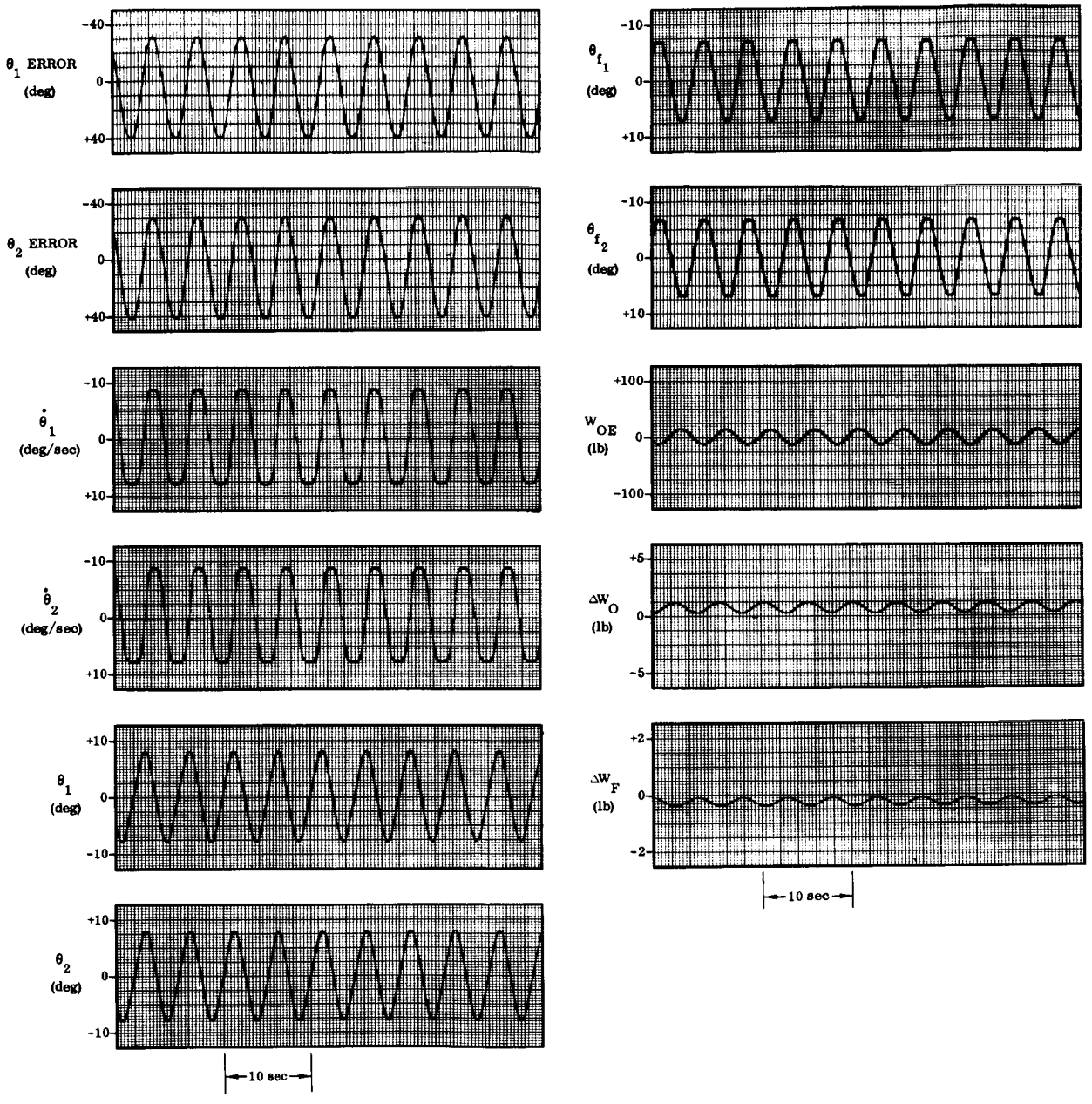

Figure 4-5. Slosh Response, Frequency = 0.2 cps, ΔW_O = 20 pounds peak-to-peak, K_V = 29 degrees, α_T = 91 ft/sec^2

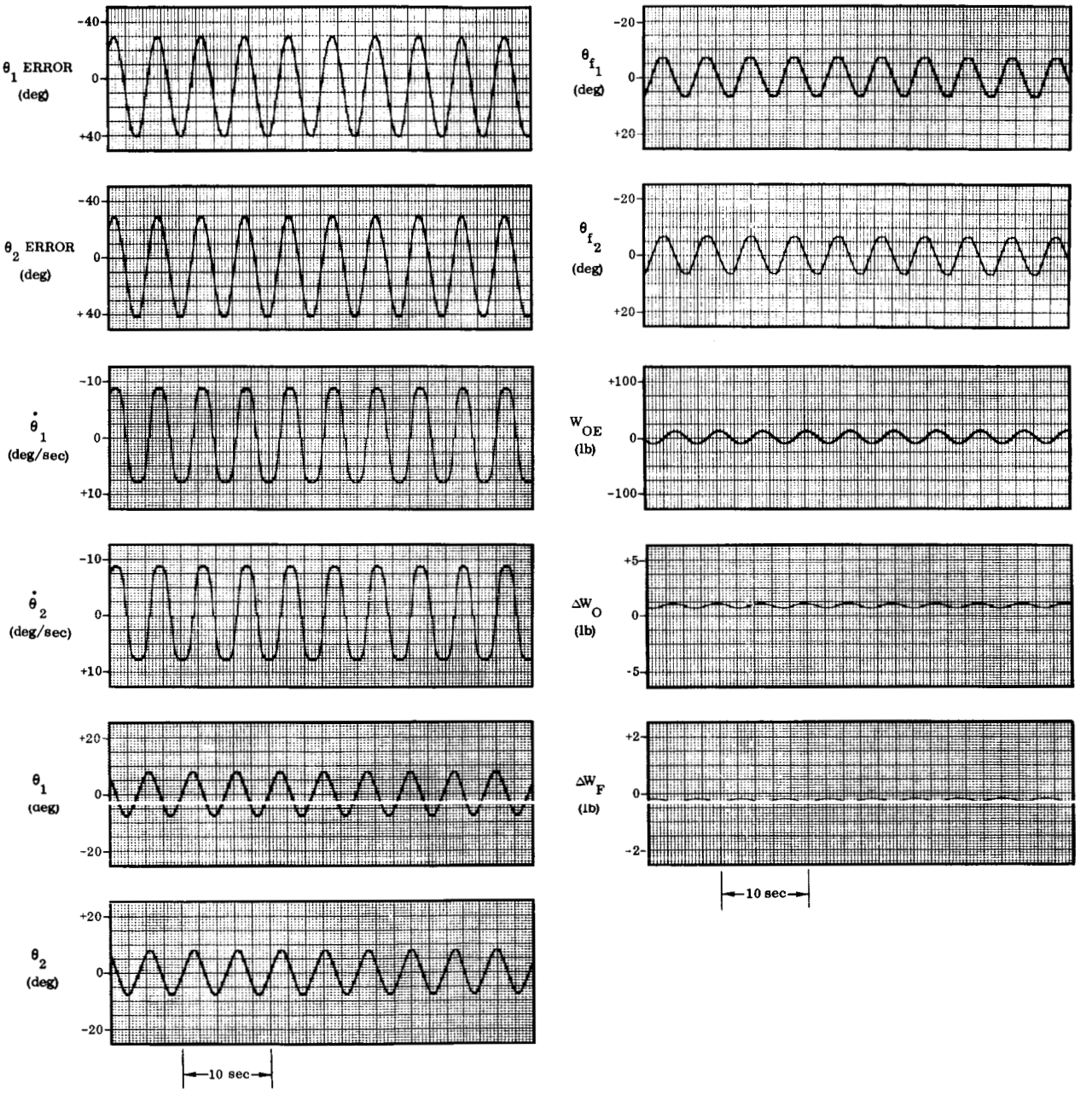

Figure 4-6. Slosh Response, Frequency = 0.2 cps, ΔW_O = 20 pounds peak-to-peak, K_V = 70 degrees, α_T = 91 ft/sec^2

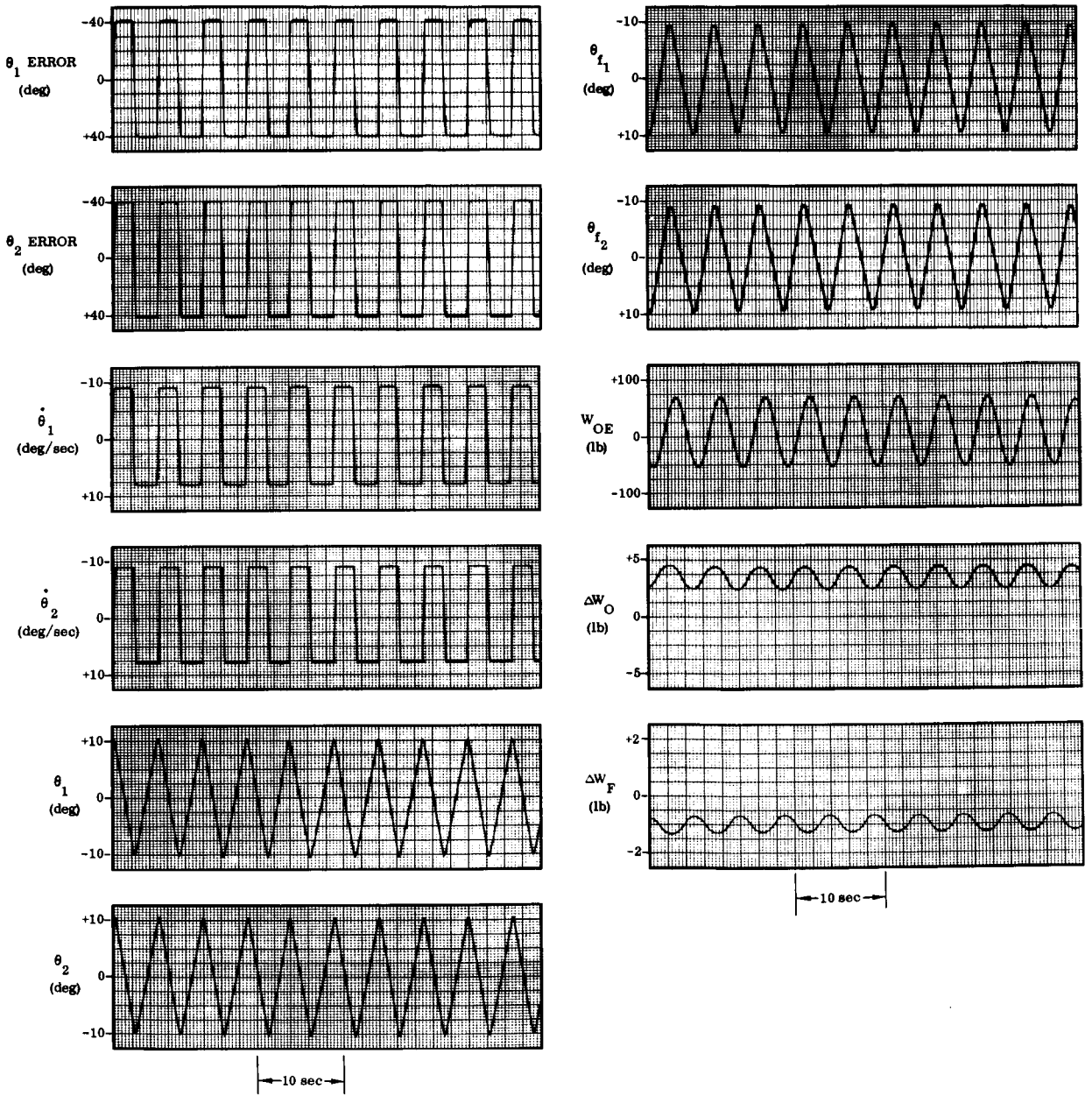

Figure 4-7. Slosh Response, Frequency = 0.2 cps, ΔW_O = 100 pounds peak-to-peak, K_V = 15 degrees, α_T = 91 ft/sec^2

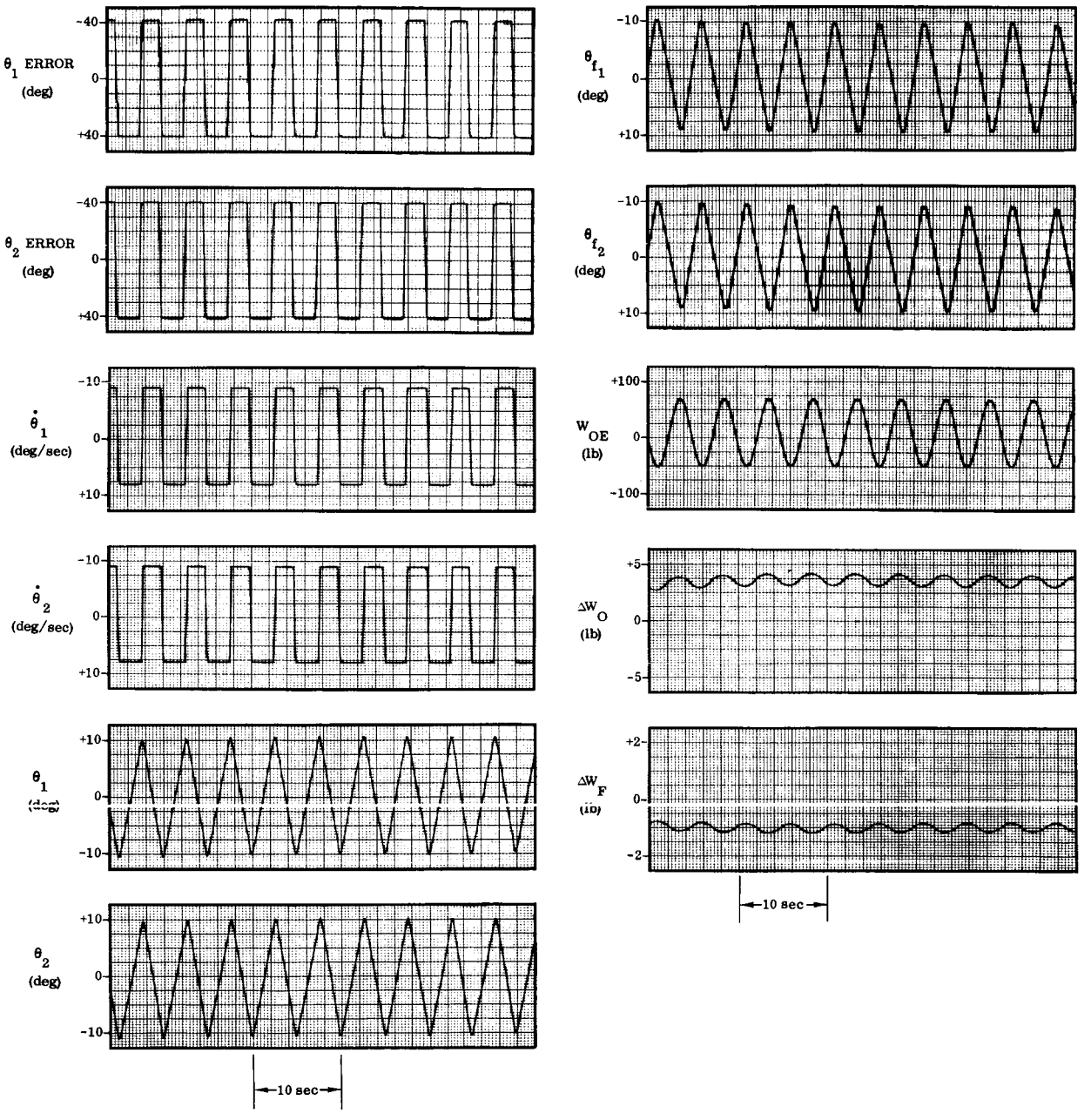

Figure 4-8. Slosh Response, Frequency = 0.2 cps, ΔW_O = 100 pounds peak-to-peak, K_V = 29 degrees, α_T = 91 ft/sec^2

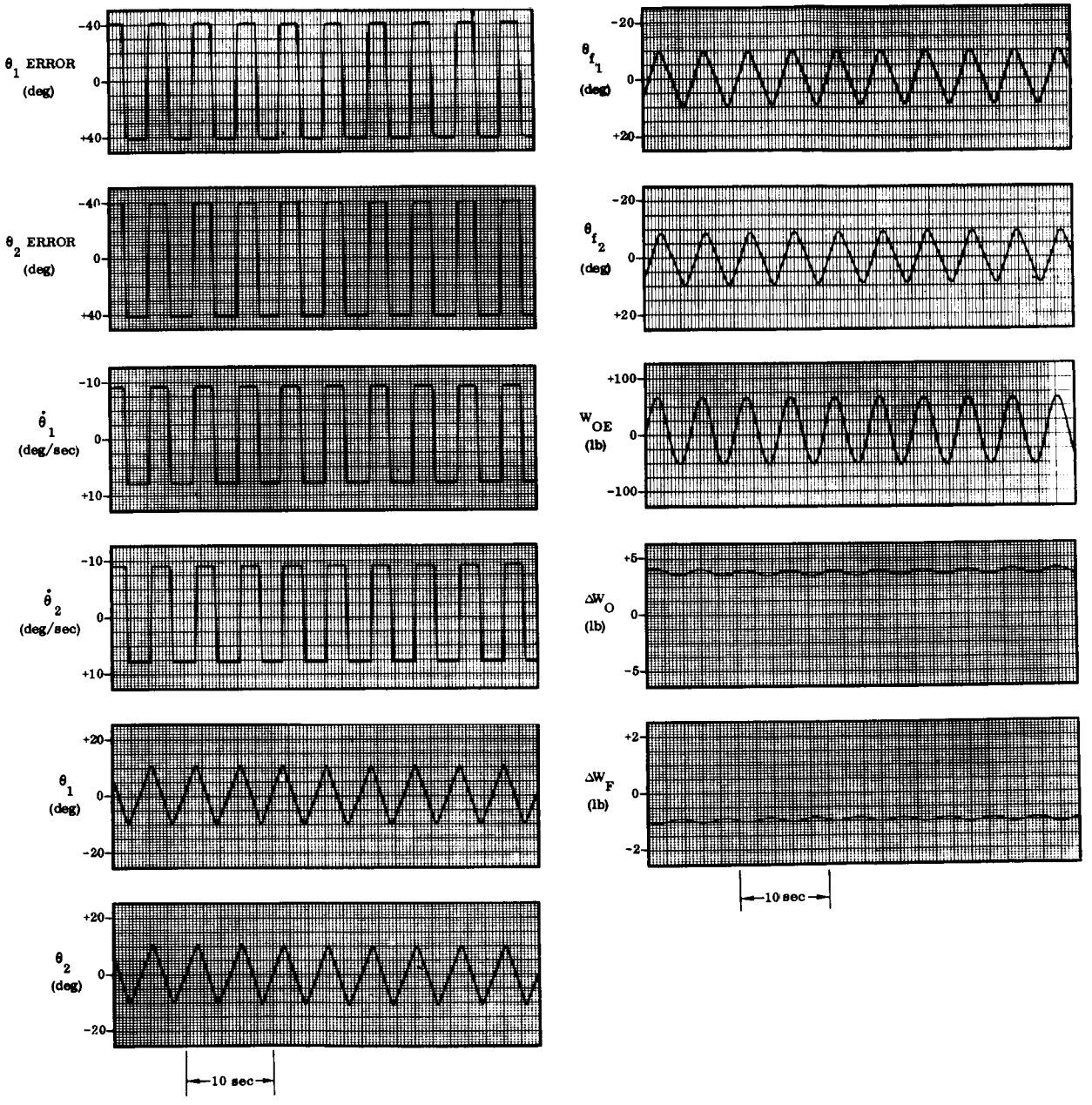

Figure 4-9. Slosh Response, Frequency = 0.2 cps, ΔW_O = 100 pounds peak-to-peak, K_V = 70 degrees, α_T = 91 ft/sec^2

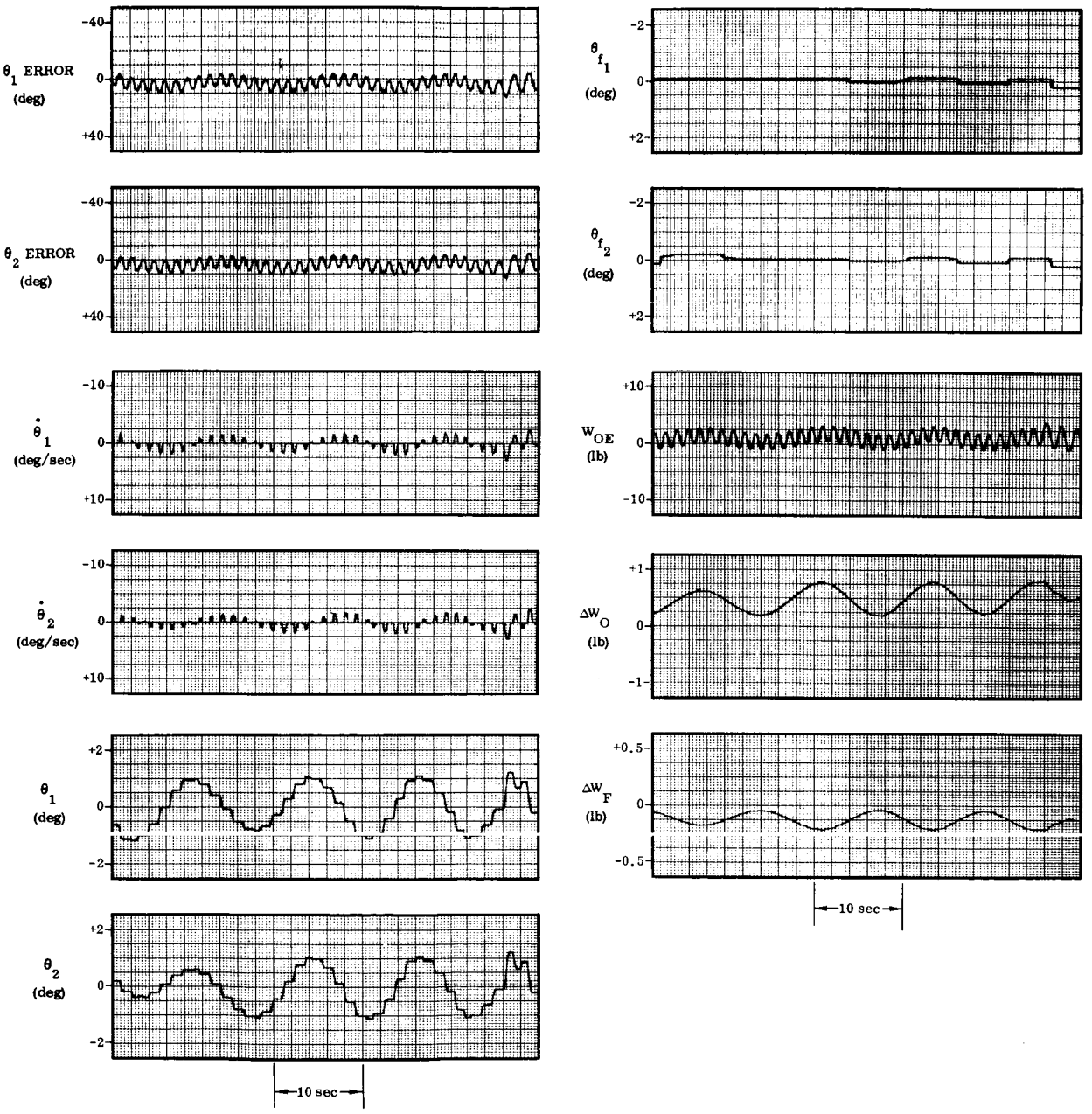

Figure 4-10. Slosh Response, Frequency = 0.8 cps, ΔW_O = 20 pounds peak-to-peak, K_V = 15 degrees, α_T = 91 ft/sec^2

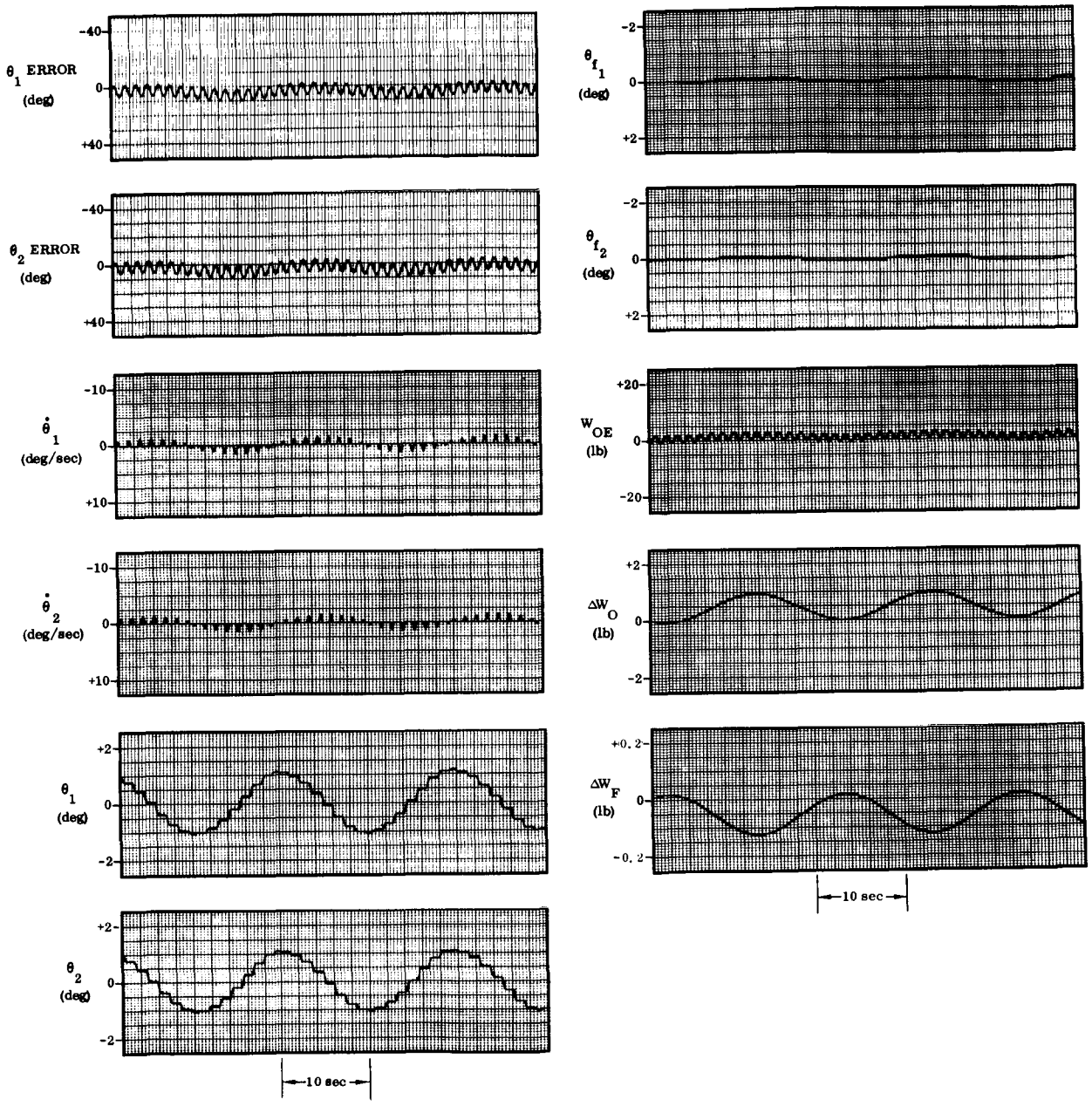

Figure 4-11. Slosh Response, Frequency = 0.8 cps, ΔW_O = 20 pounds peak-to-peak, K_V = 29 degrees, α_T = 91 ft/sec^2

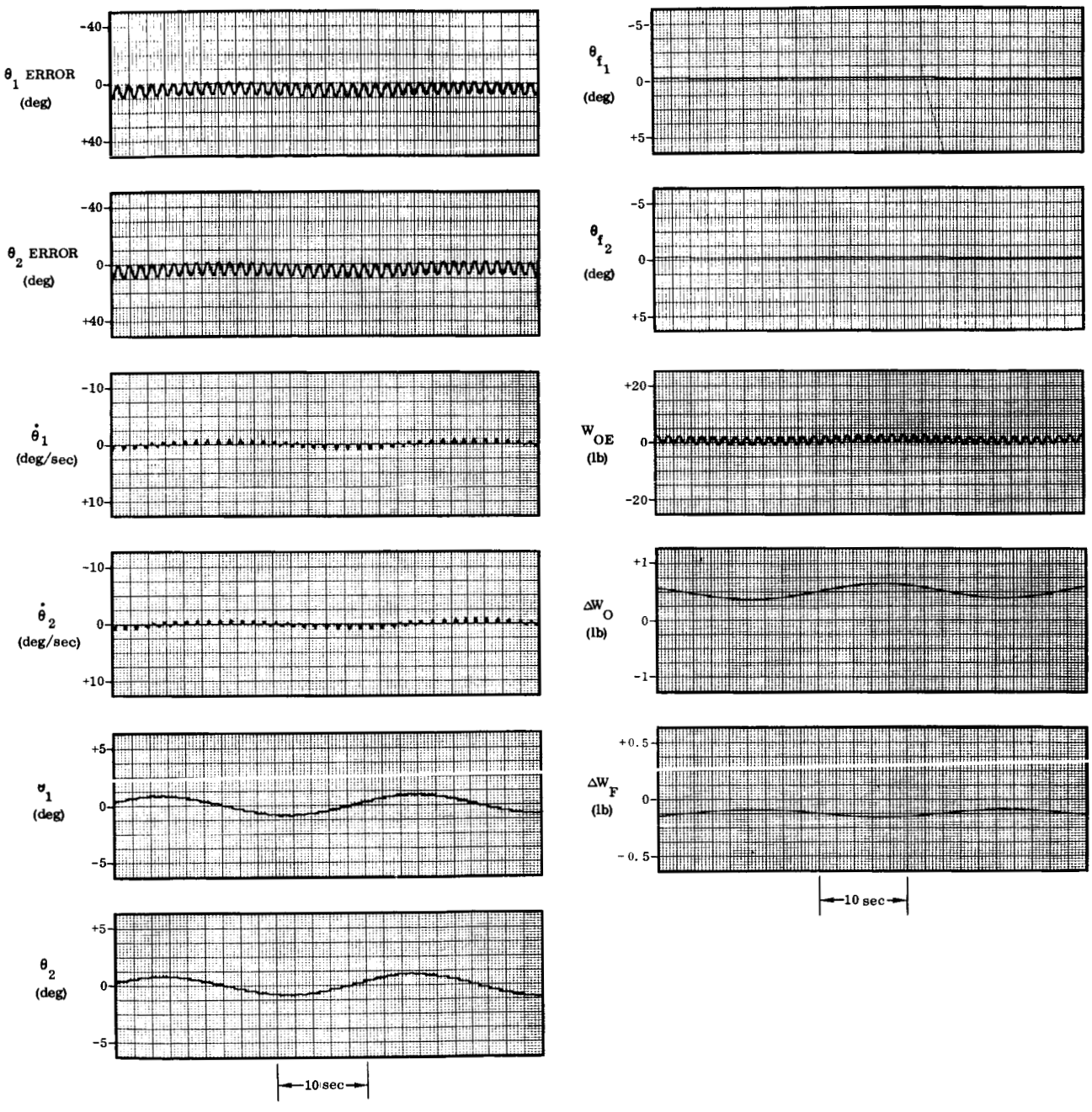

Figure 4-12. Slosh Response, Frequency = 0.8 cps, ΔW_O = 20 pounds peak-to-peak, K_V = 70 degrees, α_T = 91 ft/sec^2

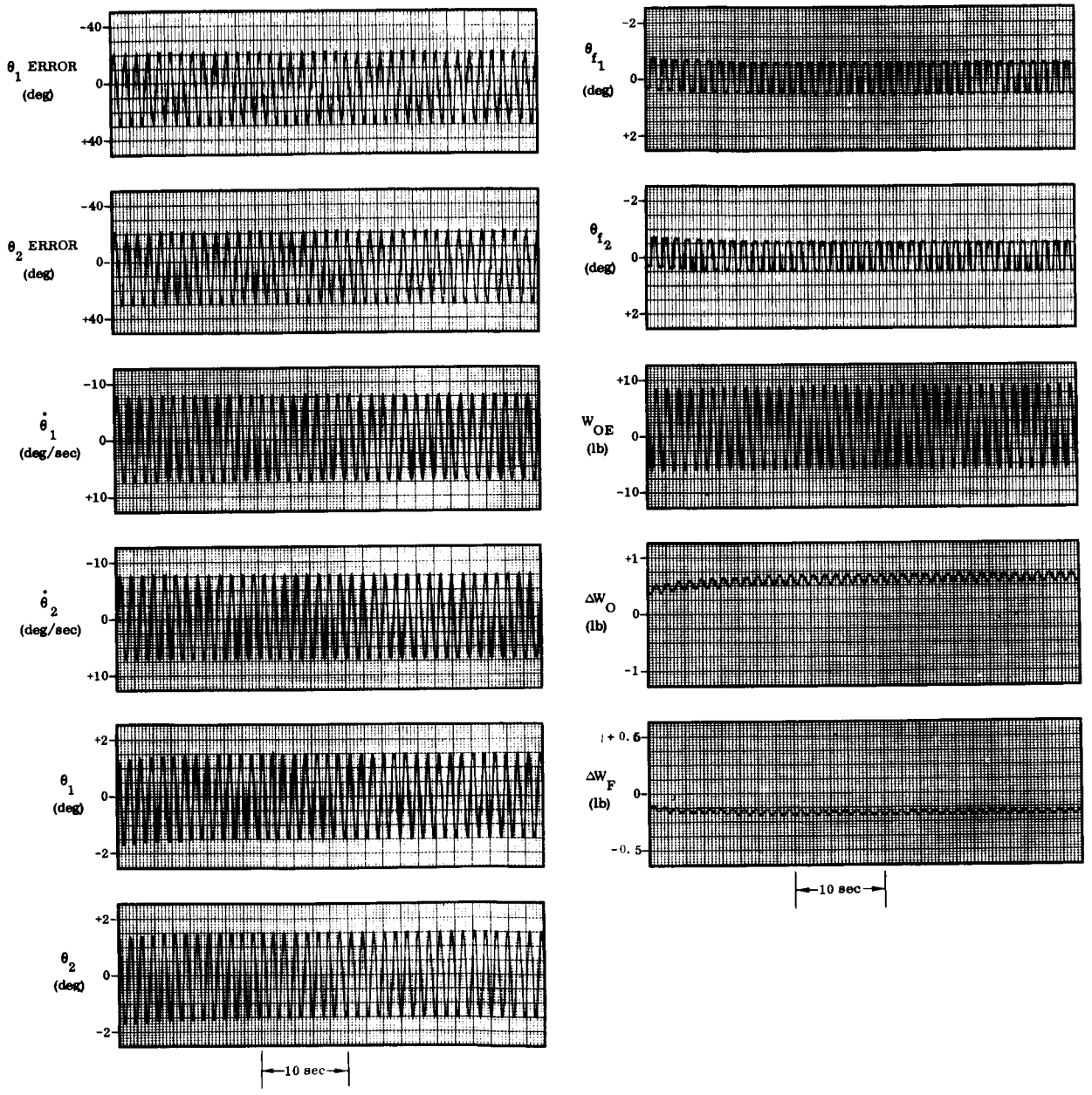

Figure 4-13. Slosh Response, Frequency = 0.8 cps, ΔW_O = 100 pounds peak-to-peak, K_V = 15 degrees, α_T = 91 ft/sec^2

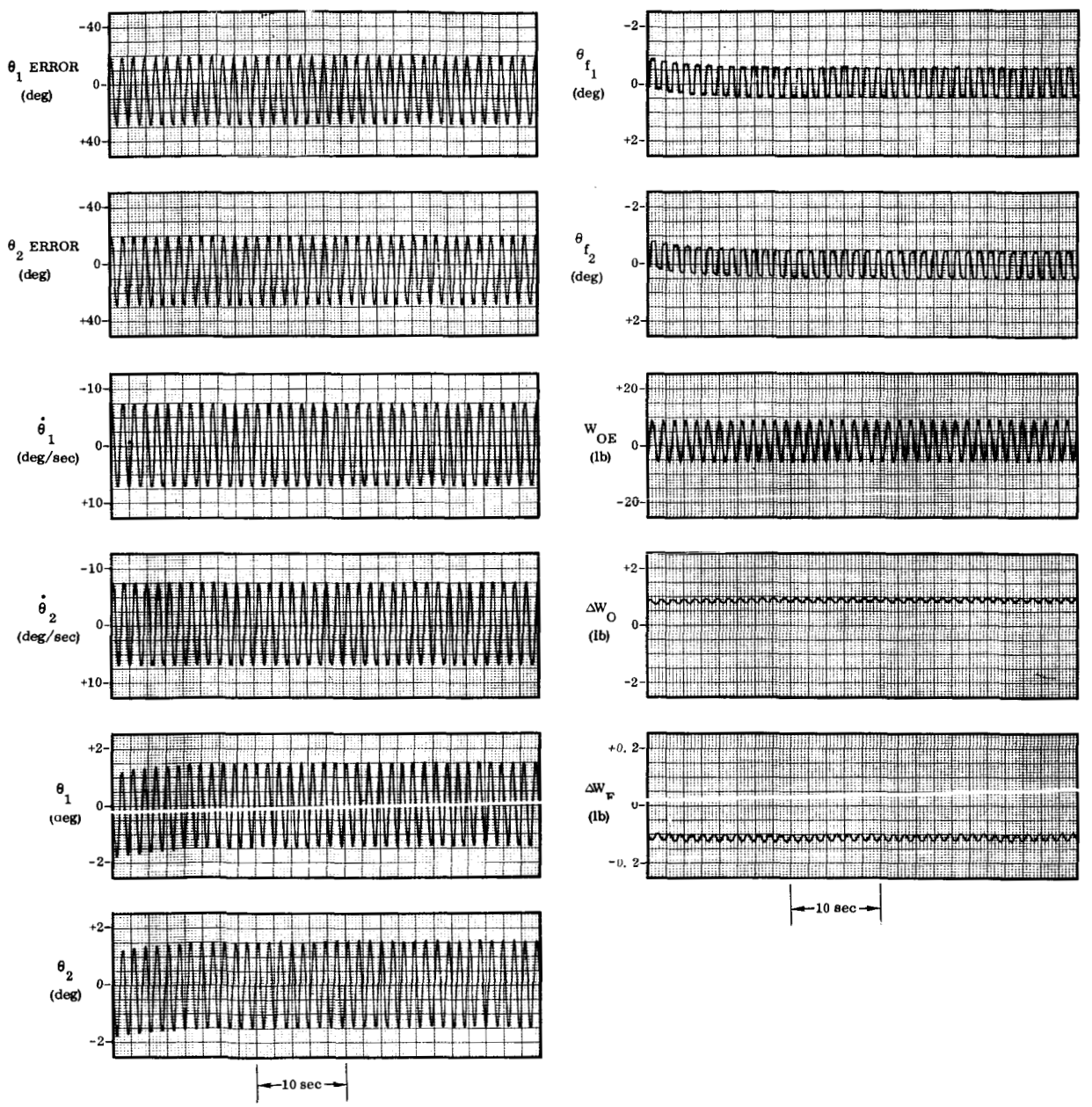

Figure 4-14. Slosh Response, Frequency = 0.8 cps, ΔW_O = 100 pounds peak-to-peak, K_V = 29 degrees, α_T = 91 ft/sec^2

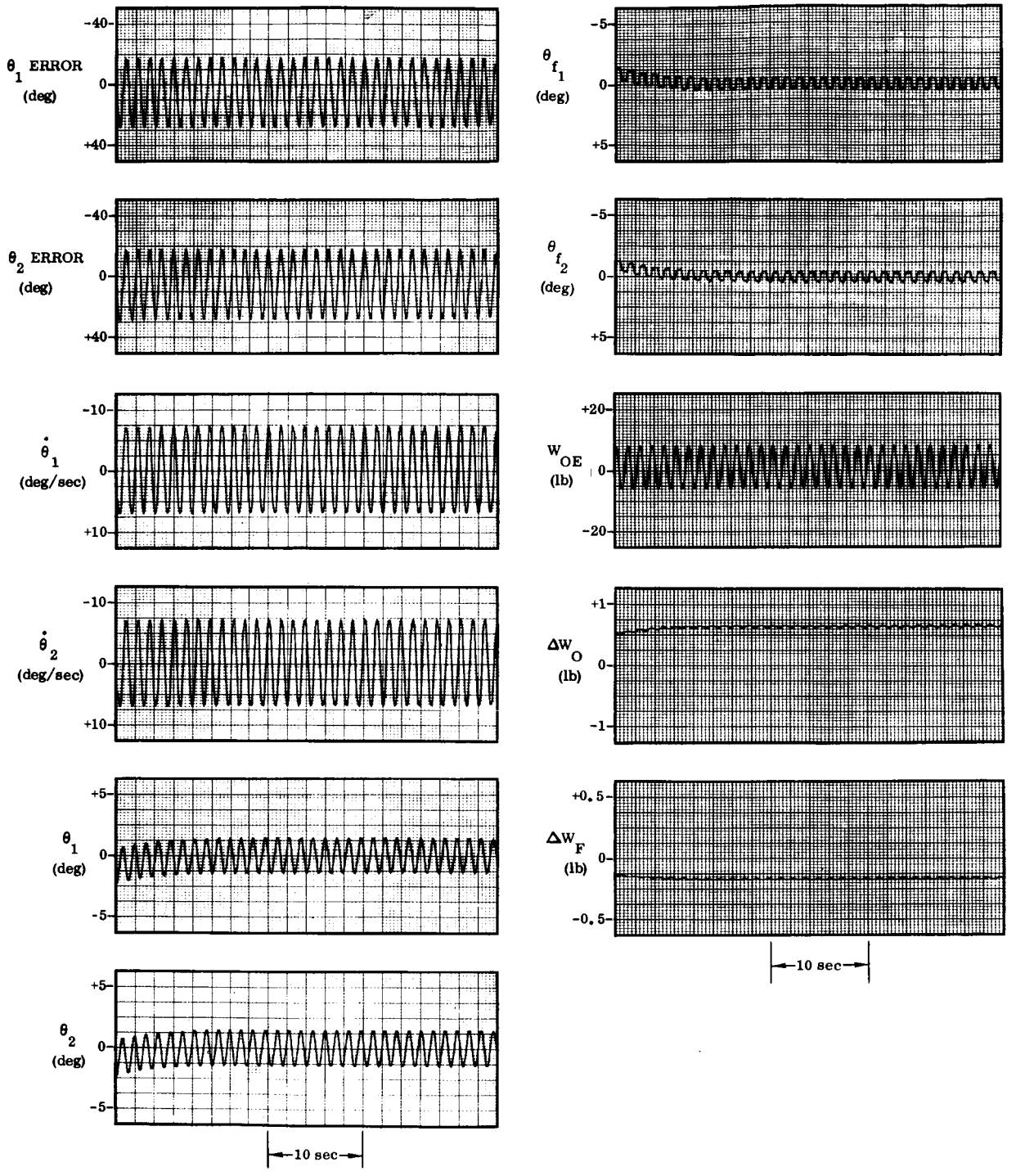

Figure 4-15. Slosh Response, Frequency = 0.8 cps, ΔW_O = 100 pounds peak-to-peak, K_V = 70 degrees, α_T = 91 ft/sec^2

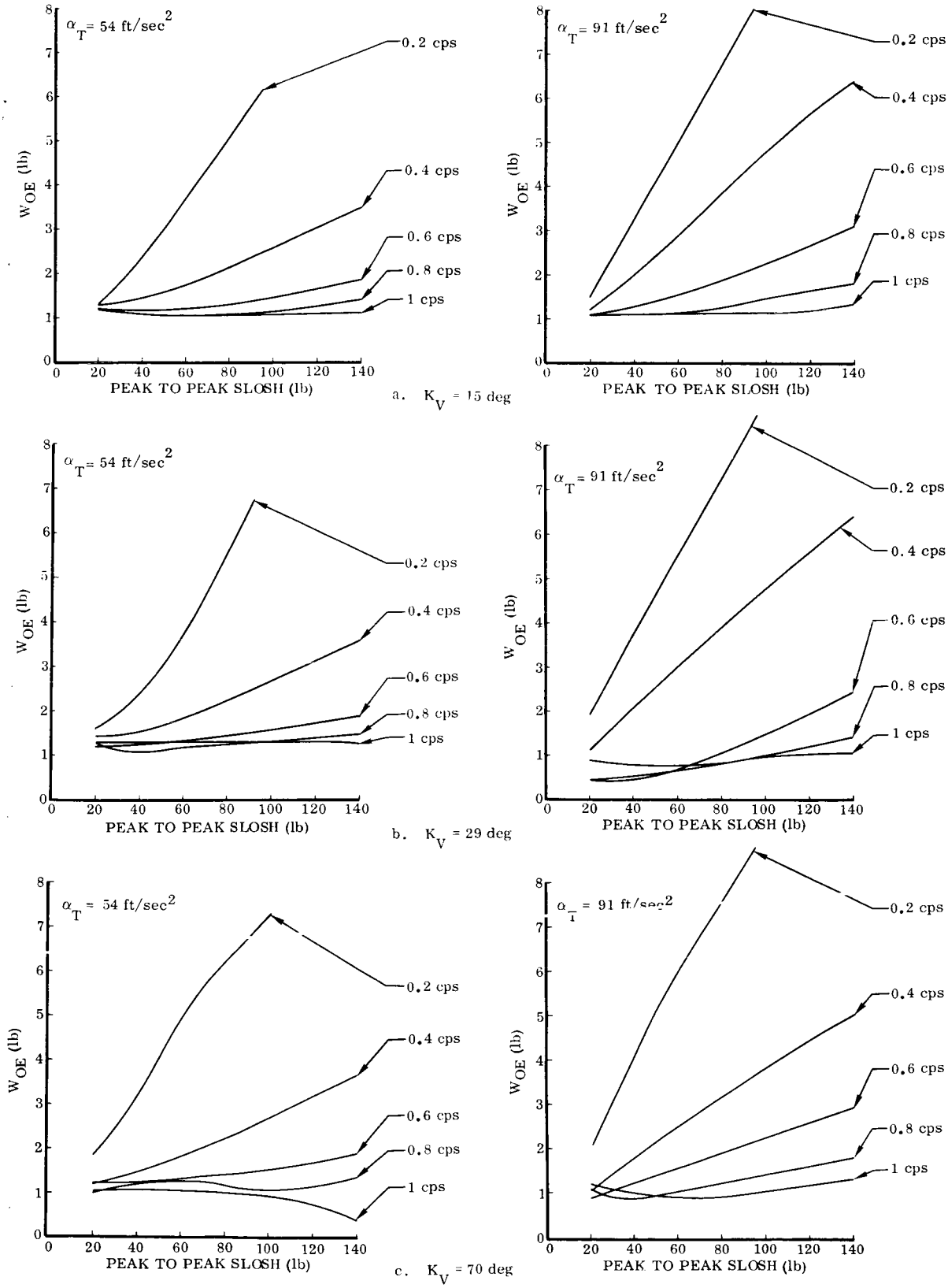

Figure 4-16. Steady-State Error Due to Sloshing

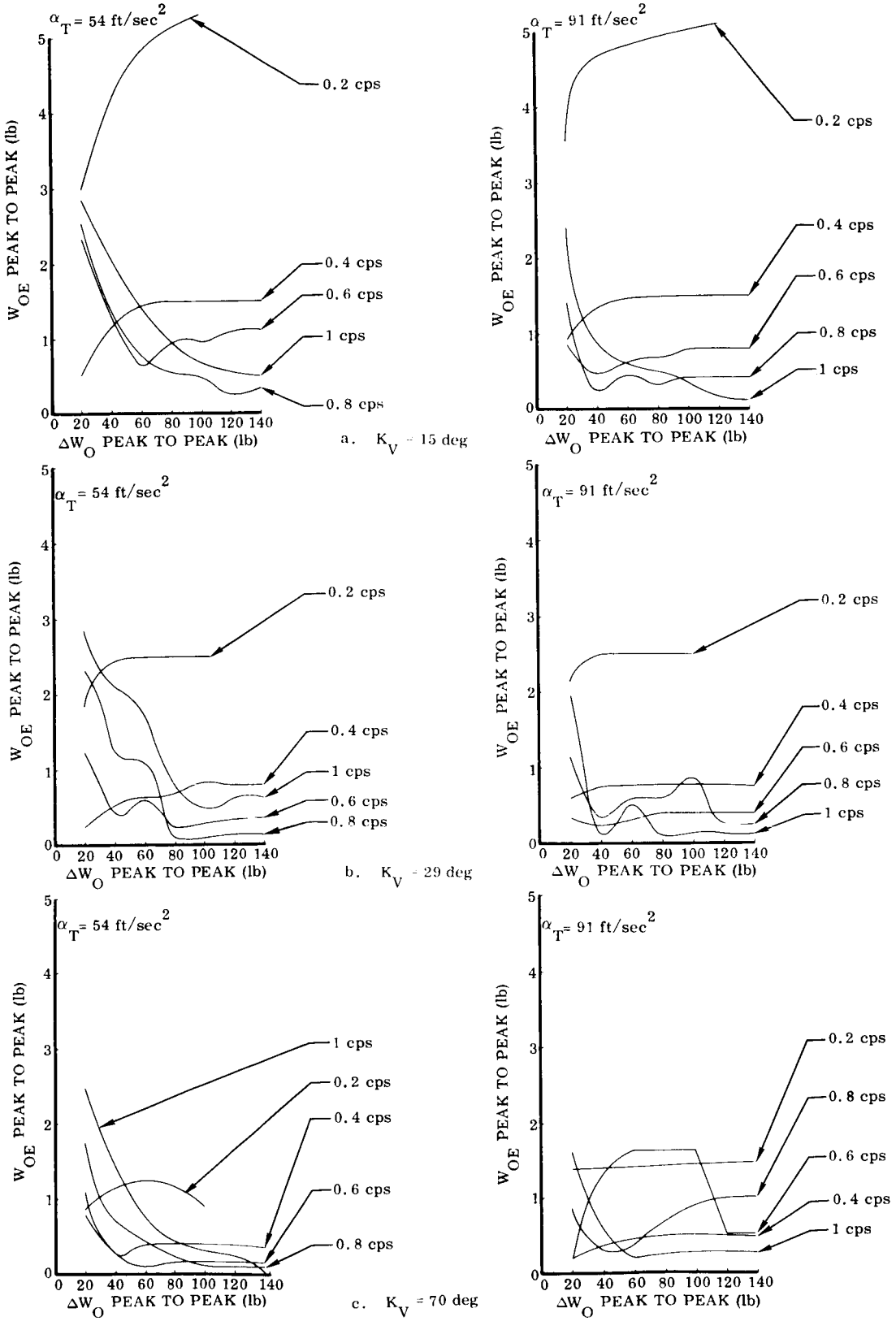

Figure 4-17. Time-Dependent Errors Due to Sloshing

SECTION 5

CONCLUSIONS AND RECOMMENDATIONS

The foregoing analyses of the system dynamic behavior show the propellant utilization control system to be stable, except for a small-amplitude limit cycle, and relatively insensitive to relatively large (100 percent) changes in the system gains. It will operate successfully in the presence of propellant sloshing more severe than expected during flight. The steady-state errors due to propellant sloshing, engine calibration errors, and limit cycle behavior are well within the maximum allowable error of 150 pounds of equivalent oxidizer error. The system response, while slow, is adequate in view of the long operating times (on the order of 200 seconds). Thus the system is felt to be adequate for correcting the expected errors in tanking ratio and mixture ratio.

The present technique of changing the valve position feedback gain to compensate for changes in the engine characteristics (thus keeping the outerloop gain fixed) does not accomplish the design objective of maintaining fixed response characteristics. While this is not serious at present operating gains, a change to higher loop gains, as a means of reducing the steady-state error, will cause a greater change in the system response for changes in K_θ. A better method would be to vary the summing bridge-amplifier gain, K_A, to compensate for changes in the valve/engine flow rate gain. This would enable the system to operate at higher gain levels while maintaining a fixed stability margin.

SECTION 6

REFERENCES

1. J. S. Hahn, Propellant Utilization Control for Centaur, Engine Systems Group Memo 962-4-386, 14 August 1964.

2. D. L. Witt, RL 10A-3 Linear Engine Simulation for GD/A Propellant Utilization Study, Pratt & Whitney Aircraft Interoffice Correspondence, 8 May 1963.

3. F. G. Rivinius, Centaur Inertia-Tube Stillwells, General Dynamics/Astronautics Report RAC ZZ-D-63-012, 26 December 1963.

4. F. W. Herman, AC-7 "Green Door", Control Dynamics Group Memo CD-64-002 BD, 8 January 1964.

5. B. Dove, Centaur Tank Volumes Versus Station Numbers, AC-6 and ON. Centaur Weights Group Memo CW 64-20, 20 February 1964.

6. D. R. Lukens, Engine Mixture Ratio Limit Setting for Early Centaur Vehicles, Dynamics Group Memo AD-1510, 12 March 1962.

7. L. R. Kaszas, Flight Dynamics and Control Analysis of the Centaur Vehicle (Atlas/Centaur AC-4), General Dynamics/Astronautics Report GD|A-DDE64-077, October 1964.

8. H. Goldstein, Classical Mechanics, Addison-Wesley Publishing Co., Inc., 1953.

9. W. D. Beye, Servo Positioner - Propellant Utilization Vehicleborne Specification, General Dynamics/Astronautics Drawing 55-04335, 2 July 1963.

APPENDIX A

DERIVATION OF SYSTEM EQUATIONS

A.1 PROBE/TANK EQUATIONS. A single probe/tank system is shown in Figure A.1-1.

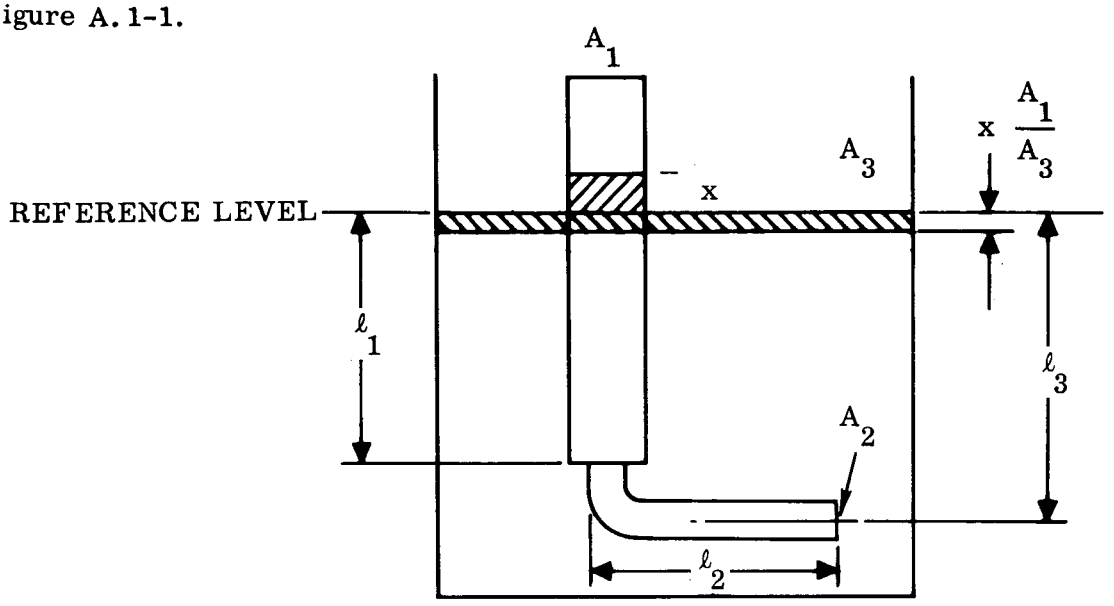

Figure A.1-1. Single Probe/Tank System

The equation of motion for this system can be derived from Lagrange's equations. (See Reference 8.)

$$\frac{d}{dt}\left(\frac{\partial L}{\partial \dot{q}_i}\right) - \frac{\partial L}{\partial q_i} = Q_i \qquad \text{(A.1-1)}$$

$$L = T - V \qquad \text{(A.1-2)}$$

$$T = \frac{1}{2}(\ell_1 + x) A_1 \rho \dot{x}^2 + \frac{1}{2}\ell_2 A_2 \rho \dot{x}^2 \left(\frac{A_1}{A_2}\right)^2 + \frac{1}{2}\left(\ell_3 - x\frac{A_1}{A_3}\right) A_3 \rho \dot{x}^2 \left(\frac{A_1}{A_3}\right)^2 \qquad \text{(A.1-3)}$$

$$V = \frac{1}{2} A_1 x^2 \alpha_T \rho - \frac{1}{2} A_3 x^2 \left(\frac{A_1}{A_3}\right)^2 \alpha_T \rho \qquad \text{(A.1-4)}$$

$$\frac{\partial L}{\partial \dot{x}} = (\ell_1 + x) A_1 \rho \dot{x} + \frac{\ell_2 A_1^2 \rho \dot{x}}{A_2} + \frac{\ell_3 A_1^2 \rho \dot{x}}{A_3} - \frac{A_1^3 \rho x \dot{x}}{A_3^2} \qquad \text{(A.1-5)}$$

$$\frac{d}{dt}\left(\frac{\partial L}{\partial \dot{x}}\right) = \rho A_1 \left\{ \ddot{x} \left[\ell_1 + \ell_2 \frac{A_1}{A_2} + \ell_3 \frac{A_1}{A_3} + x \left(1 - \frac{A_1}{A_3}\right)^2 \right] + \dot{x}^2 \left[1 - \left(\frac{A_1}{A_3}\right)^2 \right] \right\} \quad \text{(A.1-6)}$$

$$\frac{\partial L}{\partial x} = - A_1 \alpha_T \rho x \left(1 - \frac{A_1}{A_3}\right) \quad \text{(A.1-7)}$$

For small perturbations these equations can be simplified as follows:

$$A_1 = 4.9 \text{ in.}^2 \quad \text{(A.1-8)}$$

$$A_3 = 11,300 \text{ in.}^2 \quad \text{(A.1-9)}$$

$$\frac{A_1}{A_3} \ll 1 \quad \text{(A.1-10)}$$

$$\therefore \left(1 - \frac{A_1}{A_3}\right) = 1 \quad \text{(A.1-11)}$$

$$\ell_1 \cong \ell_3 \quad \text{(A.1-12)}$$

$$\ell_2 \frac{A_1}{A_2} = 355 \text{ in.} \quad \text{(A.1-13)}$$

$$\ell_2 \frac{A_1}{A_2} \ll x \quad \text{(A.1-14)}$$

$$\frac{\partial L}{\partial x} = - A_1 \alpha_T \rho x \quad \text{(A.1-15)}$$

$$\frac{d}{dt}\left(\frac{\partial L}{\partial \dot{x}}\right) = \rho A_1 \left[\ddot{x}\left(\ell_1 + \ell_2 \frac{A_1}{A_2}\right) + \dot{x}^2\right] \tag{A.1-16}$$

Substituting (A.1-15) and (A.1-16) in (A.1-1) gives

$$\ddot{x} + \frac{\dot{x}^2}{\ell_1 + \ell_2 \frac{A_1}{A_2}} - \frac{Q(\dot{x})}{\rho A_1} + \frac{\alpha_T x}{\ell_1 + \ell_2 \frac{A_1}{A_2}} = 0 \tag{A.1-17}$$

The solution to (A.1-17) is known to be a second-order system with a frequency

$$\omega = \sqrt{\frac{\alpha_T}{\ell_1 + \ell_2 \frac{A_1}{A_2}}}$$

and

$$\zeta = \frac{\rho A_1 \dot{x}^2 - \left(\ell_1 + \ell_2 \frac{A_1}{A_2}\right) Q(\dot{x})}{2\rho A_1 \dot{x} \sqrt{\alpha_T \left(\ell_1 + \ell_2 \frac{A_1}{A_2}\right)}}$$

where ζ is a nonlinear damping coefficient.

$\therefore$ (A.1-17) can be written

$$\ddot{x} + 2\zeta \omega \dot{x} + x \omega^2 = 0 \tag{A.1-18}$$

If $\dot{x}$ is constant

$$\ddot{x} = 0 \tag{A.1-19}$$

$$\zeta = -\frac{x}{\dot{x}} \frac{\omega}{2} \tag{A.1-20}$$

where x is the difference between the fluid level in the tank and probe and $\dot{x}$ is the velocity of the surface of the fluid in the probe. Since x and $\dot{x}$ will always have opposite signs, (A.1-20) can be rewritten

$$\zeta = \left|\frac{x}{\dot{x}}\right| \frac{\omega}{2} \tag{A.1-21}$$

For perturbations of x and y about a nominal value, the slope of $\left|\frac{x}{\dot{x}}\right|$ can be obtained from the head loss versus velocity curves for the probes. The curve is entered at the proper velocity, and the slope of head loss per unit velocity is read off. The curves used to determine this slope are shown in Figure 2-3. The curves were determined with the system under an acceleration of 32.2 ft/sec^2. To correct the damping ratio for other accelerations, the slope of the head loss versus velocity curves should be multiplied by $\frac{32.2}{\alpha_T}$.

A.2 MOTOR TRANSFER FUNCTION. Figure A.2-1 is a block diagram of the servomotor.

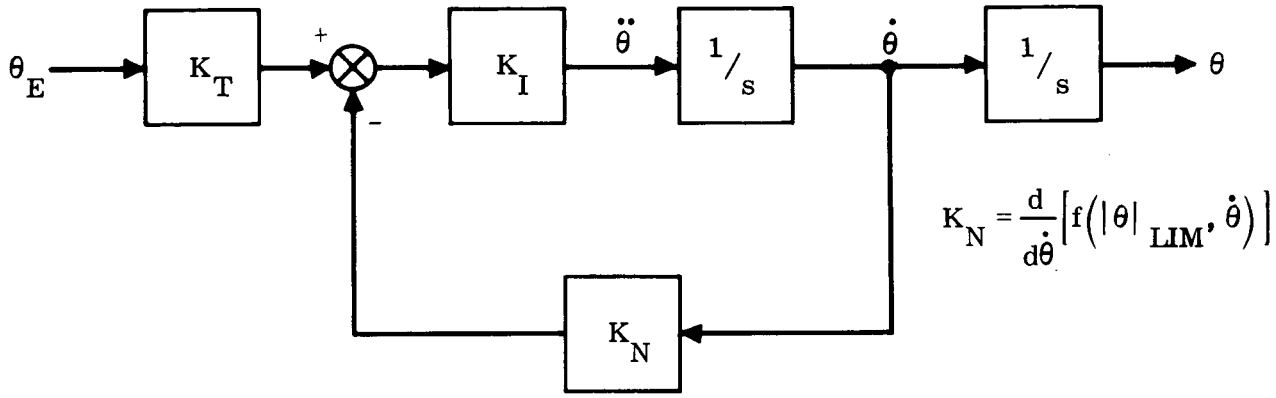

Figure A.2-1. Servomotor Block Diagram

K_N is a function of motor input voltage, motor speed, and load. For the linear stability analysis, it was assumed that the external load on the motor was zero. Figure C-1 shows a series of no-load curves for feedback torque versus valve angle velocity. Small perturbations are of interest for linear stability analysis; therefore, the value of K_N can be obtained for a particular input voltage from the slope of the curve at zero valve velocity. The block diagram of the motor can now be reduced to Figure A.2-2.

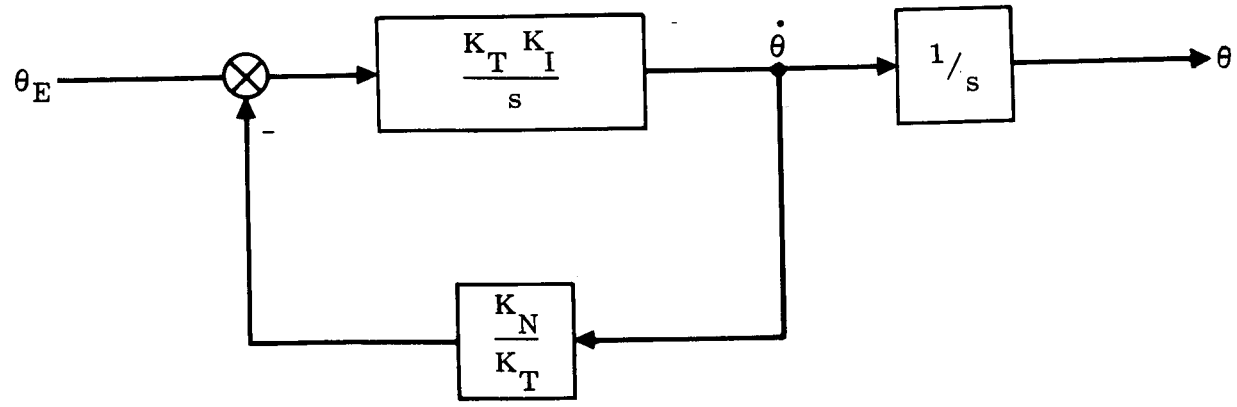

Figure A.2-2. Servomotor Simplified Block Diagram

$$\dot{\theta} = \frac{\frac{K_T K_I}{s}}{1 + \frac{K_T K_I}{s}} \theta_E \qquad \text{(A.2-1)}$$

$$\frac{\dot{\theta}}{\theta_E} = \frac{\frac{K_T}{K_N}}{\frac{s}{K_T K_I} + 1} \qquad \text{(A.2-2)}$$

Let

$$\frac{K_T}{K_N} = K$$

and

$$\frac{K}{K_T K_I} = \tau(K)$$

$$\frac{\dot{\theta}}{\theta_E} = \frac{K}{\tau(K)s + 1} \qquad \text{(A.2-3)}$$

$$\frac{\theta}{\theta_E} = \frac{K}{(\tau(K)s + 1)\, s} \qquad \text{(A.2-4)}$$

A.3 LIMIT CYCLE EQUATIONS. A limit cycle will be present in W_{OE} as a result of backlash, valve friction, and valve load. To determine analytically the amplitude and period of this limit cycle, a set of phase plane equations are derived. Several simplifications were made to facilitate writing the equations that apply during the time the oxidizer valve can move. First, the dynamics of the motor, engine flow control system, and the propellant probes are eliminated. Second, if the valve is outside the position feedback dead band, it will always move to the edge of the dead band. Third, once the valve is in the dead band, the limit cycle will occur within the dead band. Figure 3-1 is a block diagram of the simplified system. The equations relating $\dot{W}_{OE}$ to W_{OE} for the case when the valve is moving are developed in (A.3-1) through (A.3-10).

When the valve load and friction torque are greater than the motor torque resulting from W_{OE}, the valve cannot move, and $\dot{W}_{OE}$ will be constant. Equation A.3-11 gives

the value of this torque as a function of the system parameters. The limit cycle shown in Figure 3-2 can be reduced to a series of trajectories with the end conditions of one being the initial conditions for the next. The period and amplitude of the complete limit cycle will then be the sum of the individual trajectories.

The equations of $\ddot{W}_{OE}$ as a function of W_{OE} with the position feedback loop open are:

$$\dot{\theta} = -K_A K W_{OE} \tag{A.3-1}$$

$$\dot{W}_{OE} = 2\theta\left(K_O + 5 K_F\right) \tag{A.3-2}$$

$$\ddot{W}_{OE} = \dot{\theta}\, 2\left(K_O + 5 K_F\right) \tag{A.3-3}$$

$$\ddot{W}_{OE} = -K K_A \; 2\left(K_O + 5 K_F\right) W_{OE} \tag{A.3-4}$$

By multiplying both sides of (A.3-4) by W_{OE} and integrating with respect to time,

$$\ddot{W}_{OE}\, \dot{W}_{OE} = -K K_A \; 2\left(K_O + 5 K_F\right) W_{OE}\, \dot{W}_{OE} \tag{A.3-5}$$

$$\frac{\dot{W}_{OE}^{\,2}}{2} + \frac{K K_A \; 2\left(K_O + 5 K_F\right) W_{OE}^{\,2}}{2} = C \tag{A.3-6}$$

where C is the constant of integration and can be evaluated from the initial conditions on $\dot{W}_{OE}$ and W_{OE}.

The maximum amplitude limit cycle resulting in greatest W_{OE} error will occur when initial conditions on $\dot{W}_{OE}$ and W_{OE} are:

$$\dot{W}_{OE} = 2\left(K_O + 5 K_F\right)\theta_b \tag{A.3-7}$$

$$W_{OE} = 0 \tag{A.3-8}$$

Substituting (A.3-7) and (A.3-8) in (A.3-6),

$$C = 2\left(K_O + 5 K_F\right)^2 \theta_b^{\,2} \tag{A.3-9}$$

Substituting (A.3-9) in (A.3-6) and rearranging terms,

$$\frac{\dot{W}_{OE}^{2}}{4\left(K_O + 5K_F\right)^2 \theta_b^2} + \frac{K K_A W_{OE}^{2}}{2\left(K_O + 5K_F\right)\theta_b^2} = 1 \qquad \text{(A.3-10)}$$

This is the equation of an ellipse with semi-axes $2(K_O + 5K_F)\theta_b$ and

$$\sqrt{\frac{2\left(K_O + 5K_F\right)}{K K_A}}\,\theta_b .$$

The value of W_{OE} required before the valve will move is

$$\frac{f\left(\frac{\dot{\theta}}{|\dot{\theta}|}\right)}{K_A K_T} \qquad \text{(A.3-11)}$$

Therefore the amplitude of W_{OE}, $W_{OE} > 0$, is

$$\theta_b \sqrt{\frac{2\left(K_O + 5K_F\right)}{K KA}} + \frac{f\left(\frac{\dot{\theta}}{|\dot{\theta}|}\right)_+}{K_A K_T} \qquad f\left(\frac{\dot{\theta}}{|\dot{\theta}|}\right)_+ , \frac{\dot{\theta}}{|\dot{\theta}|} > 0 \qquad \text{(A.3-12)}$$

and $W_{OE} < 0$,

$$\theta_b \sqrt{\frac{2\left(K_O + 5K_F\right)}{K K_A}} + \frac{f\left(\frac{\dot{\theta}}{|\dot{\theta}|}\right)_-}{K_A K_T} \qquad f\left(\frac{\dot{\theta}}{|\dot{\theta}|}\right)_- , \frac{\dot{\theta}}{|\dot{\theta}|} > 0 \qquad \text{(A.3-13)}$$

The period is the sum of the time in the region where $\dot{W}_{OE}$ is constant plus the time of the elliptical trajectory.

From (A.3-4)

$$\text{Frequency} = \sqrt{2 K K_A\left(K_O + 5K_F\right)} \qquad \text{(A.3-14)}$$

$$\text{Time} = \frac{2\pi}{\sqrt{2 K K_A\left(K_O + 5K_F\right)}} \qquad \text{(A.3-15)}$$

$$\text{Time } \dot{W}_{OE} \text{ is constant} = \frac{f\left(\frac{\theta}{|\dot{\theta}|}\right)_+ + f\left(\frac{\theta}{|\dot{\theta}|}\right)_-}{K_A K_T \dot{W}_{OE}} \qquad \text{(A.3-16)}$$

$$= \frac{f\left(\frac{\theta}{|\dot{\theta}|}\right)_+ + f\left(\frac{\theta}{|\dot{\theta}|}\right)_-}{2\,\theta_b K_A K_T\left(K_O + 5\,K_F\right)} \qquad \text{(A.3-17)}$$

$$\text{Total period} = \frac{2\pi}{\sqrt{2\,K K_A\left(K_O + 5\,K_F\right)}} + \frac{f\left(\frac{\theta}{|\dot{\theta}|}\right)_+ + f\left(\frac{\theta}{|\dot{\theta}|}\right)_-}{2\,\theta_b K_A K_T\left(K_O + 5K_F\right)} \qquad \text{(A.3-18)}$$

APPENDIX B

ANALOG SIMULATION

Figure B-1 is a block diagram of the transfer functions used in the simulation of the propellant utilization control system. Because the electromechanical servo positioner is nonlinear even for small propellant mass ratio errors, it was simulated in detail. The engine and measurement probe transfer functions were represented by the same linearized transfer functions used in the digital stability analysis.

The first limit imposed on the system was the saturation of the amplifier feeding the equivalent oxidizer signal to the servo positioners. The servoamplifiers are limited to putting out 40 volts, which will result in the servomotor running at it's maximum no-load speed. The transfer function block labeled servo characteristics represents the loss in torque of the servomotor due to internal friction, windage, and electrical power losses.

This torque loss is a function of the motor input voltage and speed. Curves showing this functional relationship are in Figure C-1. Several other factors reduce available torque and thus the acceleration and speed of the motor. They are viscous and coulomb friction and load torques. The coulomb friction and a torque due to asymmetrical loading on the oxidizer valve due to flow through the valve are represented as a function of the sign of the motor rotation. Stops on the gear train limit valve movement. The stops are not solid but are torsional springs and are represented by a transfer function block that feeds this torque back as a load after the stop limits have been exceeded.

As stated in the main body of the report, there is backlash in the gear train. This backlash is represented in the simulation by backlash in the position feedback circuit. The values of the gain and the nonlinear functions are contained in Appendix C.

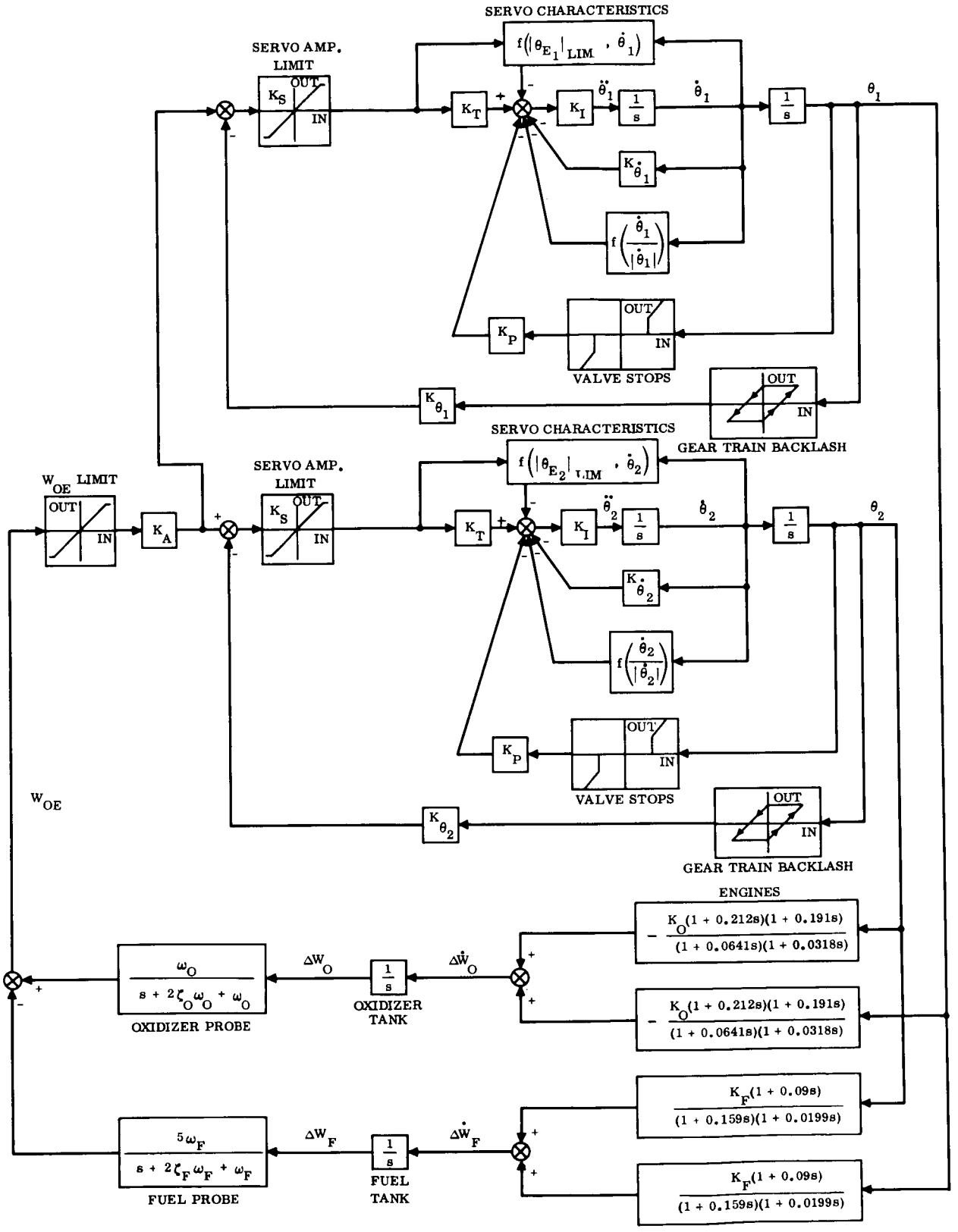

Figure B-1. Analog Simulation Block Diagram

APPENDIX C

BASIC DATA

The basic data used for both the analog and digital studies were obtained or calculated from information contained in References 1, 5, and 9. Methods of calculating ω and ζ values of the probes are included in Appendix A.1.

α_T (ft/sec^2)	DEPTH OF PROPELLANT COVERING PROBES (inches) OXIDIZER	FUEL
54	26.7	63.4
91	10.7	16.9

NO INERTIA TUBES

α_T (ft/sec^2)	ω_O (rad/sec)	ζ_O (N.D.)	ω_F (rad/sec)	ζ_F (N.D.)
54	4.5	0	3.19	0
91	10.1	0	8.03	0

INERTIA TUBES

α_T (ft/sec^2)	ω_O (rad/sec)	ζ_O (N.D.)	ω_F (rad/sec)	ζ_F (N.D.)
54	1.4	0.547	1.25	0.546
91	1.85	0.46	1.71	0.443

K_V (degrees)	K_O (lb/sec/deg)	K_F (lb/sec/deg)	K_θ (volts/deg)
15	0.0698	0.024	0.142
29	0.036	0.01053	0.0735
70	0.0149	0.00437	0.0302

K_A	0.06 volts/pound W_{OE}
Servoamplifier limit	40 volts
Summing bridge-amplifier limit	± 5 volts
K_S	50 volts/volt

Gear ratio		3200:1
Backlash		1 degree between feedback potentiometer and valve shaft

Constants referred to gear train output shaft

K_T		7.64 in.-lb/volt
$K_{\dot{\theta}}$		2.69 in.-lb/deg/sec
K_P		150 in.-lb/deg
K_I		9.3 deg/sec^2/in.-lb
$f\left(\frac{\dot{\theta}}{\lvert\dot{\theta}\rvert}\right)$	$\frac{\dot{\theta}}{\lvert\dot{\theta}\rvert} > 0$	60 in.-lb
	$\frac{\dot{\theta}}{\lvert\dot{\theta}\rvert} = 0$	30 in.-lb
	$\frac{\dot{\theta}}{\lvert\dot{\theta}\rvert} < 0$	0 in.-lb
$f\left(\lvert\theta_E\rvert_{LIM}, \dot{\theta}\right)$		See Figure C-1

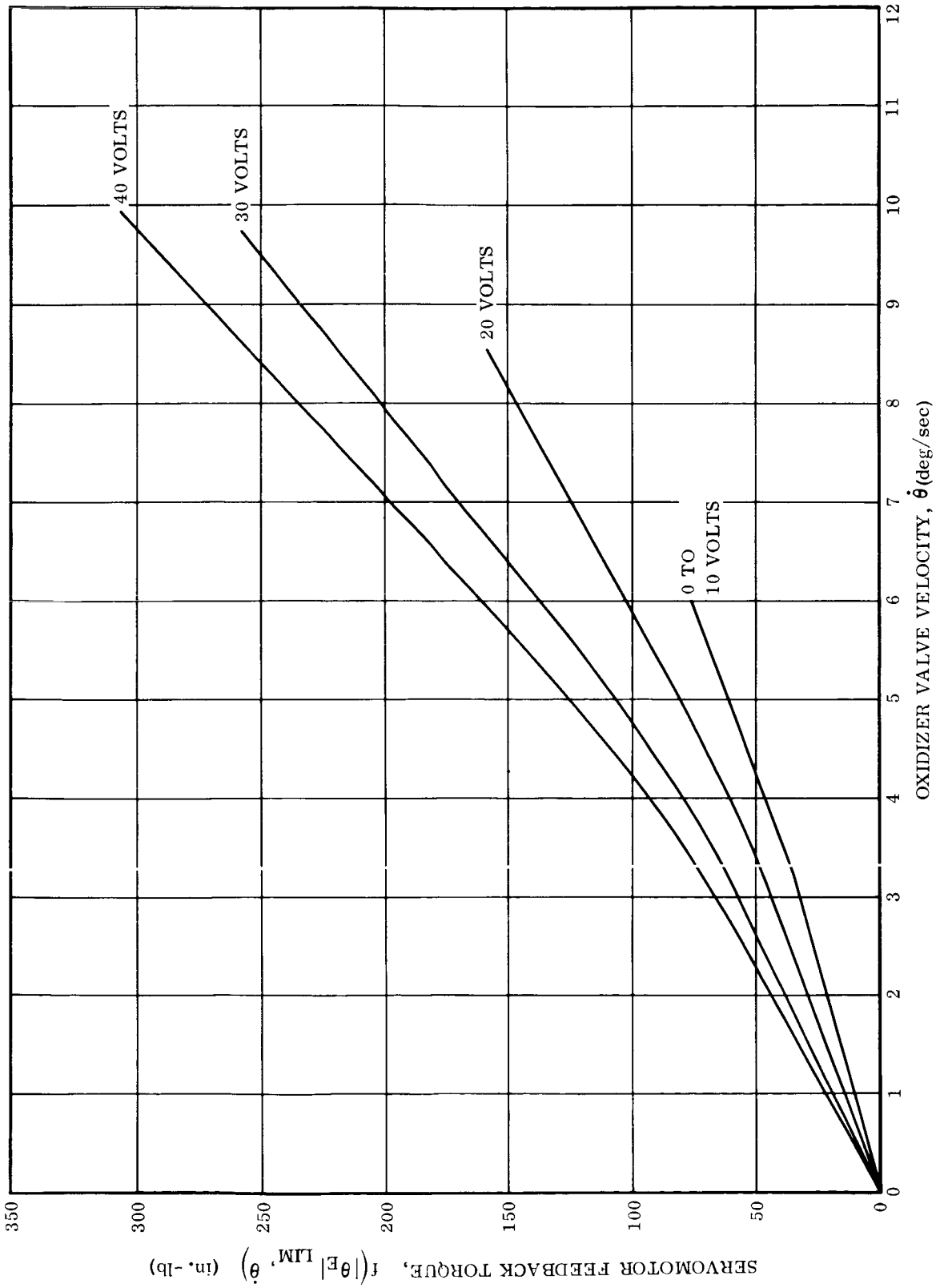

Figure C-1. Servomotor Feedback Torque